Schweizerische Eidgenossenschaft
Confédération suisse
Confederazione Svizzera
Confederaziun svizra

Department of the Environment,
Transport, Energy and Communication DETEC

Swiss Federal Office of Energy SFOE
Energy Research and Cleantech

Final report

ENHANCE

Next Generation Photovoltaic Performance

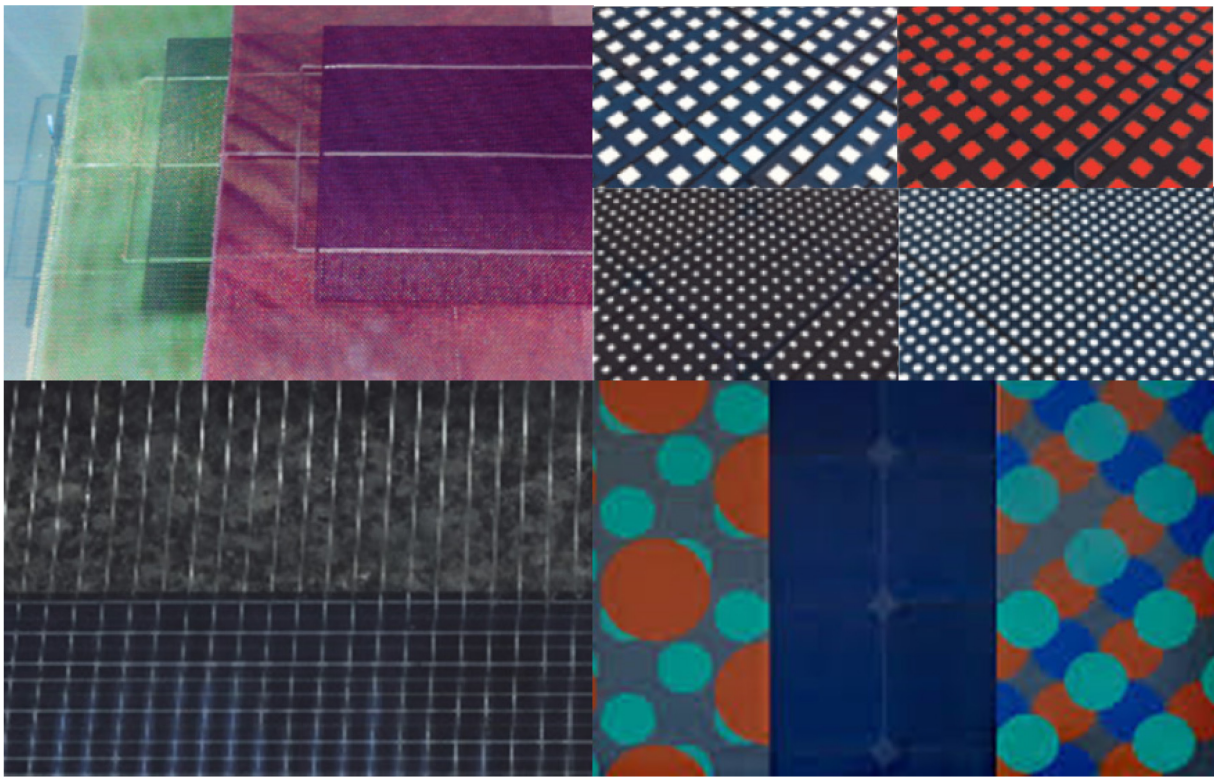

Selection of pictures from different manufacturers and R&D projects (top: Smart-Flex, PV Construct, bottom: Meyer Burger, HSLU)

University of Applied Sciences and Arts
of Southern Switzerland

SUPSI

Date: 8.11.2019

Place: Canobbio

Publisher:
Swiss Federal Office of Energy SFOE
Research Programme Photovoltaics
CH-3003 Bern
www.bfe.admin.ch
energieforschung@bfe.admin.ch

Co-financed by:
Scuola Universitaria Professionale della Svizzera Italiana, SUPSI
Campus Trevano, CH-6952 Canobbio
www.supsi.ch

Agent:
Scuola Universitaria Professionale della Svizzera Italiana
Campus Trevano, CH-6952 Canobbio
www.supsi.ch/isaac

Authors:
Ruben Roldan Molinero, SUPSI, ruben.roldanmolinero@supsi.ch
Gabi Friesen, SUPSI, gabi.friesen@supsi.ch
Mauro Caccivio, SUPSI, mauro.caccivio@supsi.ch

SFOE head of domain: Stefan Oberholzer, stefan.oberholzer@bfe.admin.ch
SFOE programme manager: Stefan Oberholzer, stefan.oberholzer@bfe.admin.ch
SFOE contract number: SI/501325-01

Summary

The ENHANCE project aimed to explore new test procedures and their measurement uncertainty, and to implement new equipment or adapting existing test facilities to new module structures with higher energy yields or higher esthetical value.

The main objective was to perform the indoor characterization of selected test samples, to install those outdoor and monitor them for a full year. The rest of the project was focused on the development of new tests and procedures such as the electrical characterization of the bi-facial technology according to the IEC 60904-1-2 and the angle of incidence loss analysis as described in the standard IEC 61853-2. The implementation of the first procedure represents an important milestone for the laboratory due to the great expectation that the bi-facial technology is creating in the market. The incident angle test determines the fraction of irradiance available for conversion into electric current and it represents an important contribution when rating power and energy under non-standard test condition, especially in aesthetic modules where colors and textures might have a relevant impact.

Zusammenfassung

Das Ziel des Projekt ENHANCE war es, neue Testverfahren für Photovoltaikmodule und deren Messunsicherheit zu erforschen, sowie die Erweiterung oder die Anpassung der bestehenden Testinfrastruktur an neue Modultechnologien mit höherem Energieertrag oder höher ästhetischem Wert.

Eine der Hauptaufgaben bestand darin, eine Anzahl ausgewählter Testmodule im Labor zu charakterisieren und diese dann Outdoor zu installieren und mindestens ein Jahr lang zu überwachen. Der Rest des Projekts konzentrierte sich auf die Entwicklung neuer Testverfahren, wie z. B. die elektrische Charakterisierung bifazialer Module gemäß IEC 60904-1-2 und die Analyse der Einfallswinkelverluste gemäss der Norm IEC 61853- 2. Auf Grund der hohen Erwartungen, welche die Bifazial-Technologie auf dem Markt geschaffen hat, stellt die Implementierung des ersten Verfahrens einen wichtigen Meilenstein für das Labor dar. Der Einfallswinkeltest bestimmt den Anteil der Bestrahlungsstärke, der zur Umwandlung in elektrischen Strom zur Verfügung steht, und stellt somit einen wichtigen Beitrag zur Bewertung von Leistung und Energie unter nicht standardmässigen Testbedingungen dar, insbesondere bei ästhetischen Modulen, bei denen Farben und Oberflächenstruktur einen relevanten Einfluss haben können.

Contents

1 Introduction

An increasing number of new modules are reaching the market promising either higher energy yields or added value due to aesthetics appearance. This is the case of bi-facial technology that claims up to 40% gain in energy yield or novel module architectures, including: active front layers for coloured modules, colour-treated glasses, anti-reflection coatings, colour-tuning thin film layers, micro-pattern techniques, coloured encapsulants or back sheets, new glass structures, anti-soiling coatings, semi-transparent cells, multi-functional module substrates, back or front serigraphy, anti-glare treatments, etc.

Many of these module concepts integrate advanced c-Si concepts with higher efficiencies or lower manufacturing costs in order to be market competitive. The most relevant and implemented technologies are: hetero-junction (HJT) and Passivated Emitter Rear Contact (PERC), which can be based on either n-type or p-type with mono or multi c-Si and are also being manufactured as bi-facial cells.

The motivation of the ENHANCE project is for the Swiss accredited PV laboratory to assess the potential impact that the measurement uncertainties might have on the cost-benefits analysis of the technologies. The project activities cover both indoors and outdoors tests and focuses on the main Key Performance Indicators (KPI) in photovoltaics. The power rating is explored indoor including the new framework of the standard IEC 60904-1-2 for bifacial modules and the performance ratio and energy yield analysis is assessed within an outdoor measurement campaign.

2 Work carried out and results achieved

2.1 Modules for Test Cycle 13

Background:

In the last years, the PV market saw further growth in c-Si modules, which at the beginning of the last decade were forecast to a slow decline in favour of the cheap and promising second-generation PV. In fact, the combined decrease in c-Si prices and increase in efficiency reversed that expectation: innovative c-Si architectures that were studied since years, finally come out, such as back-contact solar cells (commercialized by Sunpower), hetero-junction c-Si (now on Suntech Pluto cells), pushing commercial module efficiencies well over 20% and introducing new challenges for reliable performance testing.

Nowadays c-Si accounts for about 90% of the share of new processed cells and modules: as a consequence, and in order to emerge, c-Si suppliers have to push towards a product diversification and further cost reduction. The main drivers are efficiency and energy yield but also aesthetics (i.e. building integration PV): new glass structures, new encapsulants and anti-soiling coatings are proposed for this purpose.

Bifacial modules have also recently appeared on the market, increasing the module efficiency thanks to light absorption from both sides of the module. The electrical performance measurement of this technology is affected by reflections from the backside: a new procedure is needed therefore to ensure testing reliability. At the beginning of this project only best-practices exist so far, since bifacial modules are out of the scope of the IEC 60904 series. A standard measurement procedure has been under discussion for the testing of the bifacial architecture of PV modules and its implementation into the IEC 61853 energy rating standard was not clear.

Scope of the project:

- To identify and procure modules for a new outdoor measurement campaign (Ciclo 13) on emerging PV technologies with the focus on aesthetics and bifaciality.
- To characterise and demonstrate efficiency losses/gains of new module architectures or coatings
- To test different methodologies for the characterization of bifacial modules
- To cooperate to the development of new international standard test methods.

Results:

- A set of aesthetics modules including ceramic digital printing technology, selective filters and textured glass as different colour treatment or aesthetic appearance were studied. The colors of the tested modules ranged from red/terracotta to white/grey modules including plain color and multi-color devices. One of the modules was designed with bifacial cells.
- Plain colors in the tested modules are found to reduce the short-circuit current and respectively also the performance from 10.5% up to 45.5% depending on the color and coating thickness. The highest loss was as expected observed for the white module with completely hidden cells.
- In multi-color modules a further difference in performance was expected due to the contribution of possible mismatching effects from the designed patterns. Despite the completely different patterns and colors of the 2 modules from the same manufacturer representing Swiss cantonal flags, a relative difference in performance of just 5% was however found. A careful planning of the artistic design was found to be the key point to minimize the module's mismatch losses.

- The selective filter used in the white module reflects and diffuses the visible spectrum, leading to a loss in short-circuit current, but it should also improve the thermal performance respect to its crystalline reference device. As demonstrated in chapter 2.2, this important feature has a relevant and positive impact when modules operate under real conditions, especially on hot weather or BIPV applications with high temperatures. For P_{max} a temperature coefficient of about 7% lower respect to the transparent reference module was measured. The source of this difference in the temperature coefficient is still unclear, but since the relative difference is higher than the expected measurement uncertainty, further detailed and tailored studies are recommended. A higher measurement uncertainty due to spectral effects could to be the origin of this difference.
- The test infrastructure at SUPSI PVLab was upgraded to allow for the testing of bifacial modules. The single side irradiance method as described in the standard IEC 60904-1-2 was therefore introduced. The ISO17025 accreditation of the new test procedure is under preparation.
- SUPSI participated in the first international proficiency testing on the electrical performance of bi-facial modules at the standard test conditions, as set in the IEC 60904-1-2 standard for bifacial modules.
- A set of 4 different bifacial modules were characterised before being installed in the field. The multi-color textile style module with heterojunction bifacial cells, part of the colored module batch, was here also measured showing a bifaciality above 1, due to the performance loss on the front side due to the color coating.
- In general, it was observed that the smaller customized modules with less than 20 cells in series and high capacity solar cells integrated, requires a careful optimization of the measurement procedures leading to much longer measurement times when measuring with our high quality and short-pulse flasher rated as A+A+A+ according to the IEC 60904-9 standard. An optimisation of the test equipment and procedures for customized modules is therefore envisaged for the future to make the measurements more cost effective.

2.1.1 Selection of PV modules

An increasing number of new modules are reaching the market promising added value due to better building integration or aesthetics. The customers of this type of products generally seeks for a complete architectural solution all over the world and they normally require the manufacturer to provide a high amount of resources through a complete interdisciplinary team of experts working on the realization of individual customer ideas. This singularity makes difficult for the retail customer the procurement of a reduced number of modules with high aesthetic integration.

The PV modules participating in this measurement campaign have been provided by our industry partners. They are prototypes aiming to the development of characterisation methods and to analyse specific losses mechanisms. They do not represent the latest state of the art and are not provided for the sake of benchmarking.

The selected modules integrate advanced c-Si concepts with higher efficiencies or lower manufacturing costs in order to be market competitive, being hetero-junction (HJT) and passivated emitter rear contact (PERC) the most relevant technologies to be analysed. Table 1 lists the main features of the modules considered in the measurement campaign, where bi-facial modules with HJT technology are also considered. A set of c-Si reference modules with the same or compatible cell technology have been added for the sake of inter-comparison. Some manufacturers have also provided extra spare modules.

Label	**Cell Technology**	**Features**
14-I03-B7	poly c-Si	Commercial reference module
14-I03-C1	HJT	Commercial reference module
14-I03-A2	IBC	Commercial reference module
C13-E1	mono c-Si PERC	Transparent reference module (C13-D1)
C13-D1	mono c-Si PERC	White appearance - hidden cells
C13-C1	HJT, bifacial	Multi-color textile design (terracotta/white/grey stripes)
C13-C2	HJT, bifacial	Multi-color textile design (terracotta/white/grey stripes)
C13-B1	poly c-Si	Picture printings - white background - Appenzell
C13-A1	poly c-Si	Picture printings - red background - Glarus
C13-F1	mono c-Si PERC	Terracotta appearance - opaque structured glass
C13-H1	mono c-Si	Transparent reference module (C13-I1)
C13-I1	mono c-Si	Terracotta appearance - high transparency
C13-SA2	mono c-Si	Transparent reference module (C13-SC2) - black backsheet
C13-SC2	mono c-Si	Light grey (silver) - partially hidden cells
16-074-A2	HJT, bifacial	Bifacial module
16-074-C3	HJT, bifacial	Bifacial module
16-113-A1	HJT, bifacial	Bifacial module
14-I03-C4	HJT	Commercial mono-facial reference module

Table 1: List of available colored and bifacial modules together with the different transparent mono-facial reference modules.

The colored treatments in the PV modules are provided through different technologies. The modules displayed in figure 1 are made with the ceramic digital printing technology developed by the Lucerne University of Applied Sciences and it is designed to ensure that partial shading or losses do not exceed 20%.

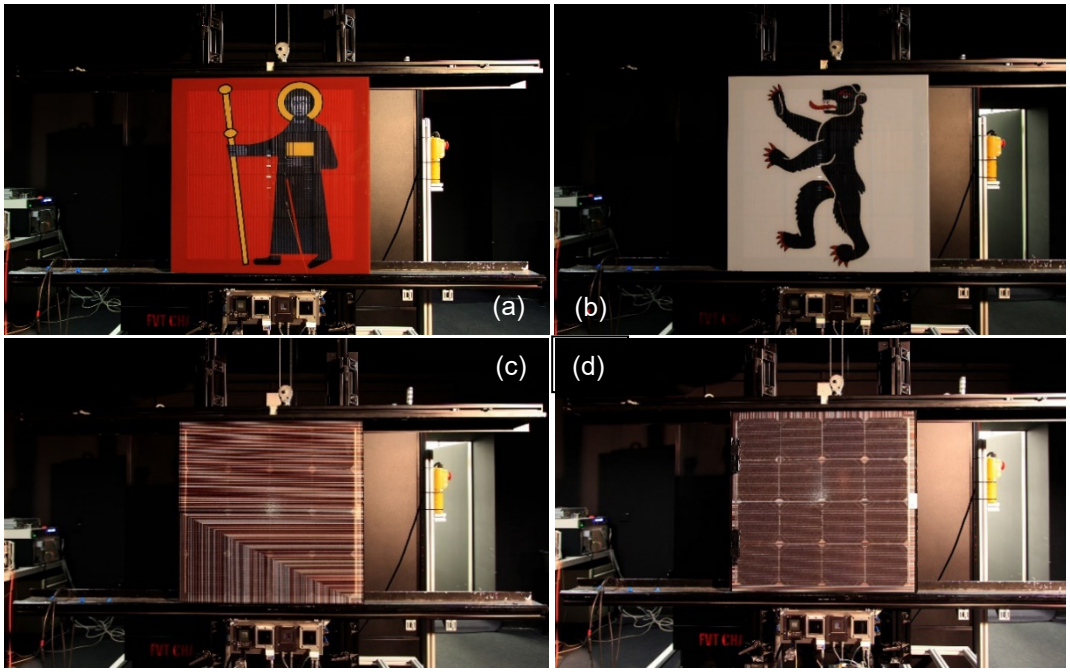

Figure 1: PV modules coloured by ceramic digital printing technology: (a) C13-A1, (b) C13-B1 and (c) & (d) front and rear side of module C13-C1.

A white module is displayed in figure 2 (right) using a selective filter in the front glass of the crystalline module which is presented in figure 2 (left) as reference module. The selective filter was developed at the Centre Suisse d'Electronique et de Microtechnique – CSEM and it is capable to reflect and diffuse the visible spectrum providing a white appearance, while the infrared part is transmitted and converted into electricity. In such a way, there is an efficiency reduction in comparison to a traditional module, but with a higher esthetical value and lower operating temperature.

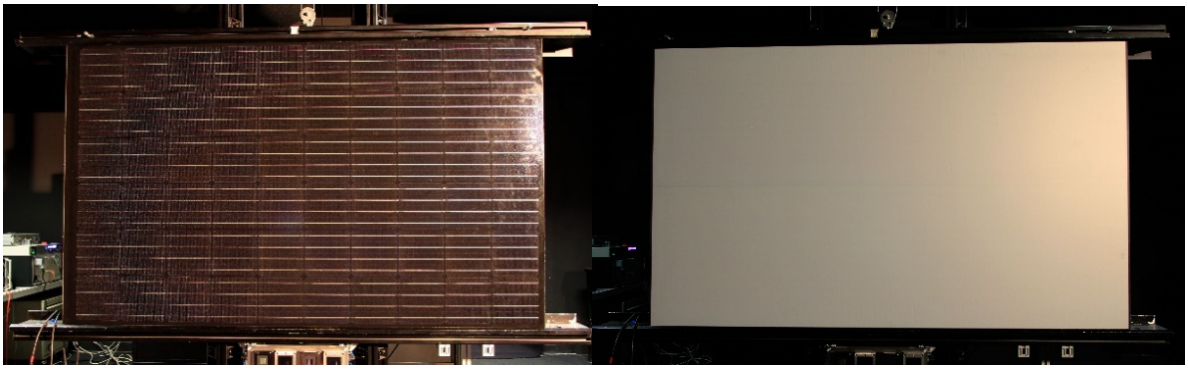
Figure 2: PV module with selective filter: (left) reference crystalline module and (right) white PV module.

Two terracotta modules with different color treatment have been provided. The first one, displayed in figure 3 (left), is also made with the ceramic digital printing technology, but compared to the cantonal flags with a uniform printing and with a prism-shaped textured glass on the front side. The second one

is shown in figure 3 (right) and is based on a mineral coating technique on glass at very high temperatures. In Figure 4, two modules employing full-surface printing with UV-resistant and translucent special inks are illustrated.

Figure 3: Two different PV modules with terracotta appearance: (left) C13-F1 module with prismatic glass and (right) C13-I1 module.

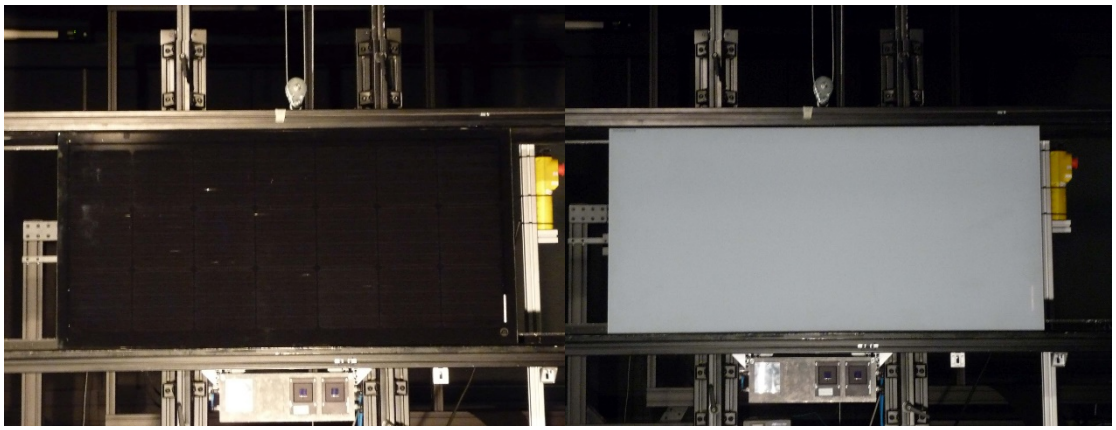

Figure 4: PV modules with full-surface printing with UV-resistant and translucent special inks: (left) C13-SA2 reference module and (right) C13-SC2 light grey module.

2.1.1 New testing challenges

The quality control and initial performance of the modules, prior to outdoor exposure, have been analyzed indoor by acquiring electroluminescence imagines, recording the IV characteristics at standard test conditions, determining the thermal coefficients and linearity through five different illumination intensities.

The electroluminescence images to control the modules have been taken by a CCD camera free of absorption filters, spectral sensitivity from 400 nm to 900 nm and resolution of 1388 x 1038 pixels. The four quadrant electronic load of the solar simulator measures the IV-curve of the device under test (DUT), the intensity of the simulated sunlight and temperatures of DUT and reference cell at the same time. The solar simulator is based on a Xe flash lamp generating a light pulse with a plateau of about 10 ms on which the spectral irradiance approximates the reference solar spectra irradiance AM1.5G with a spectral match, spatial non-uniformity and temporal instability rated as class A+A+A+ according to the IEC 60904-9 standard. The active surface of the devices under test DUTs has been mounted coplanar with a calibrated cell on either a custom designed rack, or a thermal stabilization chamber needed for the measurement of temperature coefficients. The front door of this chamber is provided with

a low iron glass door and the temperature inside ranges from 15 to 75 degrees Celsius with stability and uniformity of +/-1° and +/-1° respectively, holding up to 4 PT100 and 1 PT1000 distributed through the device under test, DUT.

2.1.2.1. Electroluminescence (EL)

The quality of the monitored PV modules throughout the identification of missing, broken or delaminated grid finger lines, cracks, low shunt resistance and improper interconnection or firing have been performed by a qualitative analysis of EL imagines measured indoors. The scope was to exclude any low quality modules or damages caused by transport before the installation on the outdoor test facility. EL images were repeated at the end of the measurement campaign.

The measurements have been performed according to the recommendations and guidelines for using EL imaging techniques to identify and assess specific failure modes of PV modules in IEA-PVPS T13-10:2018. The methods to capture electroluminescence (EL) images of photovoltaic modules, procedure to obtain quantitative metrics and guidance to qualitatively interpret the EL images are currently being standardized in IEC TS 60904-13 (for CD).

2.1.1.1. Performance at STC

The procedure for the measurement of current-voltage characteristics of the PV modules in simulated sunlight has been performed according to the IEC 60904 standard. For the sake of comparison, electrical values are normalized to the number of cells in series and cell area listed in table 3.

Label	Cells in Serie	Cells in Parallel	Cell Area (cm2)	Module Area (m2)
14-I03-B7	60	1	240.25	1.63
14-I03-C1	72	1	154.81	1.26
14-I03-A2	96	1	153.13	1.63
C13-E1	60	1	241.92	1.65
C13-D1	60	1	241.92	1.65
C13-C1	16	1	243.36	0.48
C13-C2	16	1	243.36	0.48
C13-B1	16	1	243.36	0.56
C13-A1	16	1	243.36	0.56
C13-F1	14	1	245.51	0.46
C13-H1	36	1	242.08	1.05
C13-I1	36	1	242.08	1.05
C13-SA2	21	1	242.08	0.70
C13-SC2	21	1	242.08	0.70
16-074-A2	60	1	238.56	1.64
16-074-C3	60	1	238.56	1.64
16-113-A1	60	1	242.08	1.65
14-I03-C4	72	1	154.81	1.26

Table 2: Number of solar cells connected in series and cell's area per PV module

Figure 4 compares the current density – voltage curves of the reference modules 14-I03-B7, 14-I03-C1, 14-I03-A2 and 14-I03-C4 and highlights the difference in performance between the poly-crystalline mod-

ule 14-I03-B7 and the high efficiency modules 14-I03-C1, 14-I03-A2 and 14-I03-C4, showing a significant higher Voc evaluated in approximately 13.9%. It is also important to note that there is a relevant difference in current density and fill factor between the IBC and HTJ technologies, being 7.0% and 3.5% respectively higher in 14-I03-A2 respect to 14-I03-C1. Modules 14-I03-C1 and 14-I03-C4 are manufactured by the same supplier, showing similar performance. The short-circuit current loss of the monofacial reference module 14-I03-C4 used for the analysis of performance in bifacial modules is partially compensated by its relative gain in FF, showing a final difference in efficiency of approximately ε_η = 0.4%.

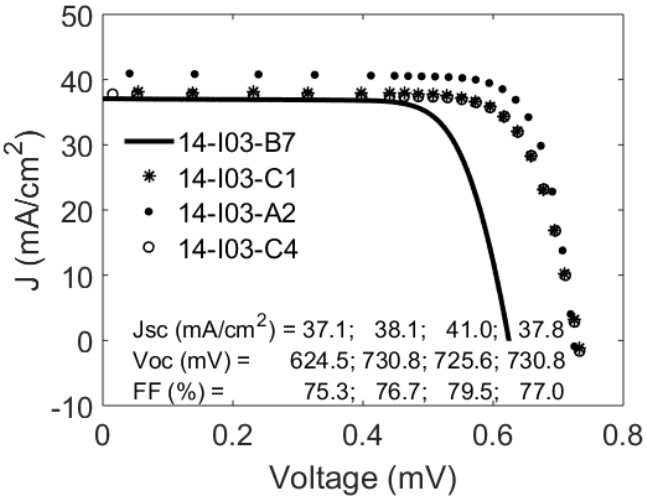

Figure 5: Comparison of current density – voltage curve of the crystalline reference modules: 14-I03-B7, 14-I03-C1, 14-I03-A2 and 14-I03-C4.

Colored modules versus transparent modules

The terracotta module with structured glass C13-F1 module was provided without reference and therefore its electrical characteristic is directly compared against our standard poly c-Si reference module 14-I03-B7 in figure 5. The 9mm thick front and prism-shaped textured color glass reduce the short-circuit current in ε_{Jsc} = 36.3%, which is slightly compensated in the overall performance by the increase of ε_{Voc} = 3.3% and ε_{FF} = 2.5%.

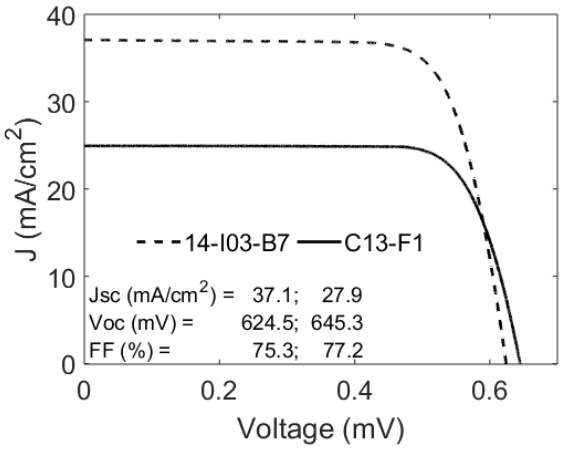

Figure 6: Comparison of current density – voltage curve of the terracotta structured glass module C13-F1 against reference 14-I03-B7.

Figure 6 compares the performance of the Appenzeller and Glarus flag (C13-B1 and C13-A1), both provided from the same manufacturer. The deviation in efficiency at STC is ε_η = 5.1%, from where the main contribution comes from the short-circuit current, ε_{Jsc} (%) = 4.1, due to the fact that the artistic design and colors are completely different. The difference in open circuit voltage and fill factor are ε_{Voc} = 0.4% and ε_{FF} = 0.6% respectively. The comparison with the reference crystalline modules yields a difference in efficiency between roughly ε_η = 30% respect to 14-I03-B7 to ε_η = 50% respect to 14-I03-A2.

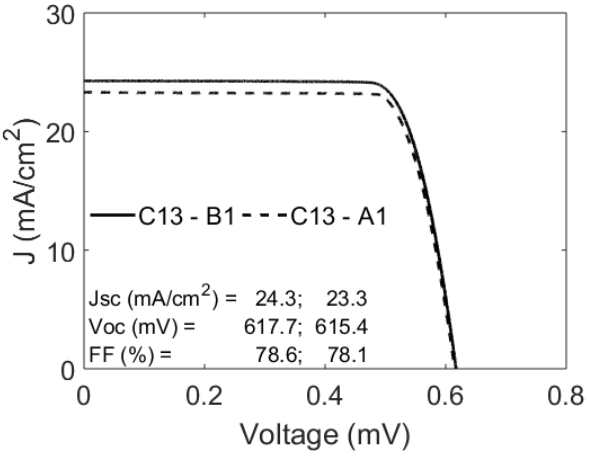

Figure 7: Comparison of current density – voltage curve of the cantonal flag modules C13-B1 and C13-A1.

The textile style modules C13-C1 and C13-C2, whose JV curves are compared in Figure 7, are highly capacitive and the methodology used to perform the measurements is based on the multi-flash technique. It is important to highlight that small size capacitive modules are difficult to measure. The measurements in a multi-flash technique should be properly distributed through the JV curve so that the characteristic parameters are properly extracted. This procedure is not always straight-forward for such small size capacitive modules and it may require a considerably time effort, especially when determining the thermal coefficients or analysis of solar intensity dependence. The industry is currently assessing the incorporation of LED simulators to face this problem, but the lack of experience introduce resistance to the penetration of the solar simulators into the market. The difference in performance at STC in the 2 modules rise up to ε_η = 7.0%. The fill factor is reduced by approximately ε_{FF} (%) = 5.2 in module C13-C1. Since the difference in short-circuit current and open circuit voltage remain relatively low: ε_{Jsc} = 0.7%, and ε_{Voc} = 1.1%, a problem with parasitic resistances might be the most likely cause of this difference in performance. Comparing the performance with a reference crystalline module, the difference in efficiency yields between roughly ε_η = 19.1% respect to 14-I03-B7 to ε_η = 40% respect to C13-B2.

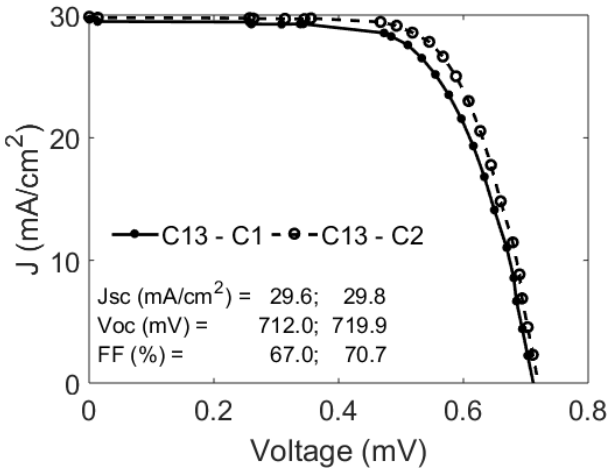

Figure 8: Comparison of current density – voltage curve of textile style modules C13 - C1 and C13 – C2.

The white module C13–D1 is compared with the provided reference C13–E1 in figure 8. The colored foil placed in front of the cells reduces the short circuit current in ε_{Jsc} = 45.5% and therefore the open circuit voltage is logarithmically reduced up to ε_{Voc} = 2.7%. The enhancement of the fill factor in ε_{FF} = 3.2% yields to an overall reduction in performance at STC in approximately ε_{η} = 45.2%

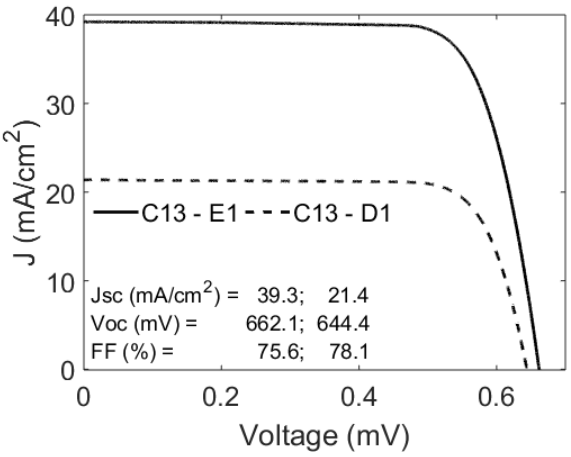

Figure 9: Comparison of current density – voltage curve of white module C13 - E1 and reference C13 – D1.

Reference module C13-SA2 is compared in figure 9 with the light grey/silver and module C13-SC2. The grey module shows a relative cell efficiency loss of $\varepsilon_{\eta} = 28\%$ respect to the reference at STC, mainly due to losses in the short-circuit current density.

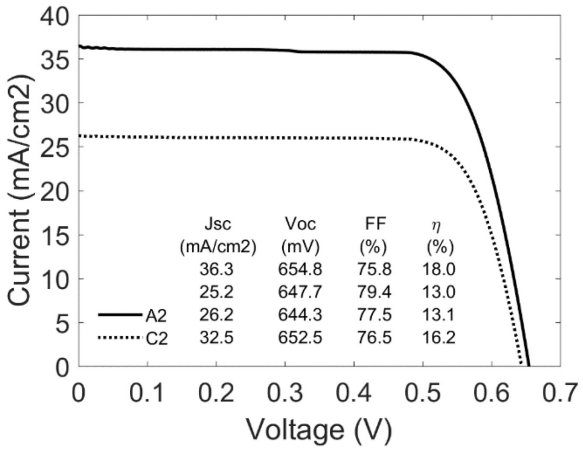

Figure 10: Comparison of current density – voltage curve of the light grey module C13 – SC2 and the reference C13 – SA2.

Bifacial versus Monofacial modules

The bi-facial photovoltaic technology is receiving growing interest on the market, with several companies commercializing bi-facial modules alongside their conventional products, based on various c-Si structures, such as p-PERC, n-PERC, HIT, IBC, etc. Indoor and outdoor current-voltage characterization of bi-facial PV modules at Standard Test Conditions (STC) are challenging, since they require careful control over the intensity and spectral distribution of the irradiance on both sides of the bifacial modules. A new dedicated international standard from the International Electrotechnical Commission (IEC) for current-voltage characterization of bifacial PV modules has been published as IEC 60904-1-2 at the end of January 2019, including all the outcomes from the technological, scientific and metrological development of recent years. The Draft Technical Specifications (DTS) IEC TS 60904-1-2 ED1 was voted and approved last 2nd November by all the voting members and it will be registered as a technical specification by 14.12.2018. The described measurement procedure has not been validated yet via ISO 17025 accredited interlaboratory comparisons, however the proficiency testing is currently being conducted and SUPSI has received the commercial size bi-facial PV modules by December 2018. In this activity, we will follow the indoor procedure and crosscheck the results with the ones obtained outdoor. Different testing approaches will be analysed and discussed within the international round – robin campaign and reported at the beginning of 2019, when the results are available.

The procedure for the measurement of the I-V characteristics of a bi-facial PV device is based on the same basic principles as in IEC 60904-1, but requires additional considerations specific to bifacial devices. The bi-faciality coefficient, φ_k, is defined as the ratio between the parameter *k* generated exclusively by the rear of the bifacial device and the one generated by the front side, where *k* refers to I_{sc}, P_{max} or V_{oc}. Figure 10 displays, the short-circuit $\varphi_{J_{sc}}$ and maximum power point $\varphi_{P_{mpp}}$ bi-faciality coefficients obtained for module 16-074A2. They were measured at different irradiance levels and the 2-σ dispersion remains below 0.5% in both cases. The mean values $\overline{\varphi_{J_{sc}}}$ and $\overline{\varphi_{P_{mpp}}}$ are listed in table4. As the difference in the mean values are below 0.5% and the measurement uncertainty in the maximum power is higher than that of the short-circuit current in the analyzed modules, the gain in power generation yielded by the bifaciality of the DUT in this work will be determined as a function of the short-circuit current bifaciality coefficient.

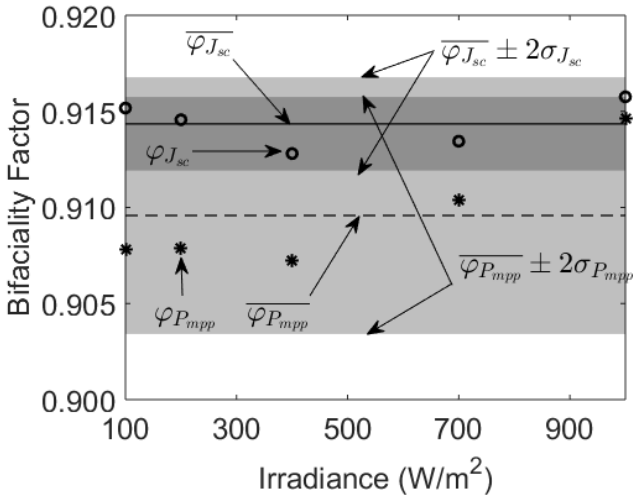

Figure 11: Comparison of short-circuit and maximum power bifaciality coefficients.

Label	$\overline{\varphi_{Jsc}}$	$\sigma_{\varphi_{Jsc}}$	$\overline{\varphi_{P_{mpp}}}$	$\sigma_{\varphi_{P_{mpp}}}$
16-074-A2	0.914	0.001	0.910	0.003
16-074-C3	0.921	0.005	0.917	0.002
16-113-A1	0.939	0.001	0.948	0.002

Table 3: Mean and standard deviation of the short-circuit current and maximum power bifacial factors measured at five different irradiance levels.

The J-V curves of the devices must be measured on the front side at equivalent irradiance levels G_{E_i} corresponding to 1000 W/m2 on the front side plus different rear side irradiance levels G_{R_i}. The equivalent irradiance levels are determined as a function of the bi-faciality coefficient φ according to:

$$G_{E_i} = 1000\ \frac{W}{m^2} + \varphi\ G_{R_i}$$

where φ is the short-circuit current bifacial factor discussed above.

At least three different equivalent irradiance levels are required for the linear interpolation that will determine the performance of bifacial devices at the specific values $G_{R_1} = 100\ W/m^2$ and $G_{R_2} = 200\ W/m^2$. In this case, as displayed in figure 11, we have performed eight measurements in the irradiance level from 100W/m2 up to roughly 1200W/m2 and determined the rate at which the short-circuit current and the efficiency change with respect to the irradiance.

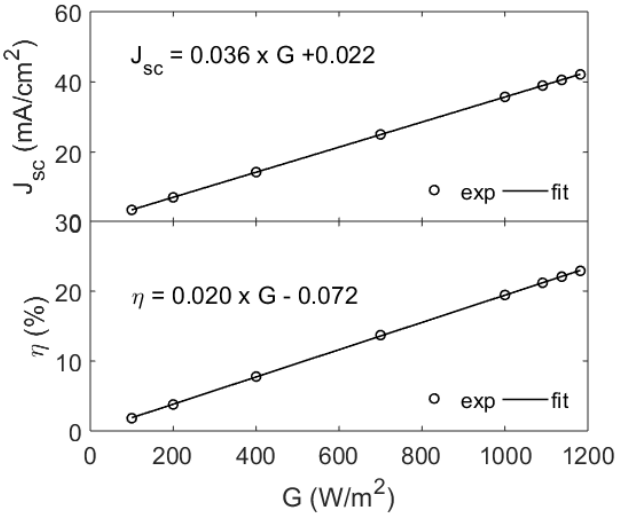

Figure 12: Determination of the rate at which the short-circuit current (top) and the efficiency (bottom) change with respect to the irradiance in the bifacial module 16-074-A2.

The traditional analysis of Variable Illumination Measurement (VIM) [Merten 1998a] in a single-diode equivalent circuit model states that the open circuit condition is achieved when the photo-generated current is compensated by the current of the diode and the illumination is sufficiently high. That is when the leakage current can be neglected and the open circuit voltage is basically determined according to

$$V_{oc} = nV_T ln\left(\frac{J_{sc}}{J_0}\right)$$

where parameters n and J_0 can be determined by a simple linear fit. Figure 12 displays the recorded measurements and fit obtained in module 16-074-A2 at irradiance values higher than 400W/m2 and table 5 compares the results between bi-facial modules. The modules were all provided by the same manufacturer and no big differences were therefore found at high irradiance levels. The rate at which J_{sc} and η change with respect to the irradiance are the same and only a certain difference has been found in the parameters of the diode in module 16-074-C3.

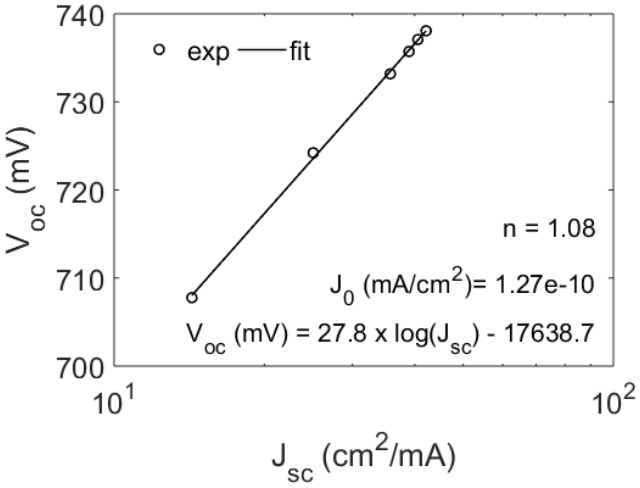

Figure 13: Determination of the diode parameters according to the analysis of variable illumination measurements in a single-diode equivalent circuit model on the bifacial module 16-074-A2

Label	$J_{sc}(G)$	$\eta(G)$	n	$J_0(mA/cm^2)$
16-074-A2	$0.036G + 0.022$	$0.020G - 0.072$	1.08	1.27e-10
16-074-C3	$0.036G + 0.014$	$0.020G - 0.098$	1.03	3.50e-11
16-113-A1	$0.036G + 0.019$	$0.020G - 0.088$	1.08	1.59e-10

Table 4: Analysis of the variable illumination measurements in bifacial modules: determination of the rate at which J_{sc} and η change with respect to the irradiance and the diode parameters in a single-diode equivalent circuit model.

2.1.1.2. Spectral mismatch correction

A PV device has a wavelength-dependent response and its performance is significantly affected by the spectral distribution of the incident radiation. The IEC 60904-7 describes the procedure to correct the mismatch between the simulated light and the reference solar spectral distribution defined in EIC 60904-3, where the irradiance of the solar simulator measured by the reference device using its calibration value G_{Sim} has to be set to the reference spectral irradiance $G_{AM1.5G}$ according to

$$G_{AM1.5G} = MMF \times G_{Sim}$$

where MMF is the spectral mismatch factor determined from

$$MMF = \frac{\int E_{AM1.5G}(\lambda) S_{ref}(\lambda) d\lambda}{\int E_{Sim}(\lambda) S_{ref}(\lambda) d\lambda} \times \frac{\int E_{Sim}(\lambda) S_{DUT}(\lambda) d\lambda}{\int E_{AM1.5G}(\lambda) S_{DUT}(\lambda) d\lambda}$$

and $E_{AM1.5G}(\lambda)$ is the reference spectral irradiance distribution, $E_{Sim}(\lambda)$ the spectral irradiance distribution of the solar simulator, $S_{ref}(\lambda)$ the spectral response of the reference PV device and $S_{DUT}(\lambda)$ the spectral response of the DUT. All integrals are performed in the full spectral range where the reference and the DUT are spectrally sensitive.

Figure 13 displays the spectral response curves of the crystalline reference modules 14-I03-B7, 14-I03-C1, 14-I03-A2 and 14-I03-C4. The results show that the high efficiency module 14-I03-A2 perform in the full sensitive range significantly better than the rest of the crystalline reference modules. However, modules 14-I03-C1 and 14-I03-C4 (both provided from the same manufacturer) perform better that 14-I03-B7 in the near infra-red, NIR, region than ultraviolet, UV.

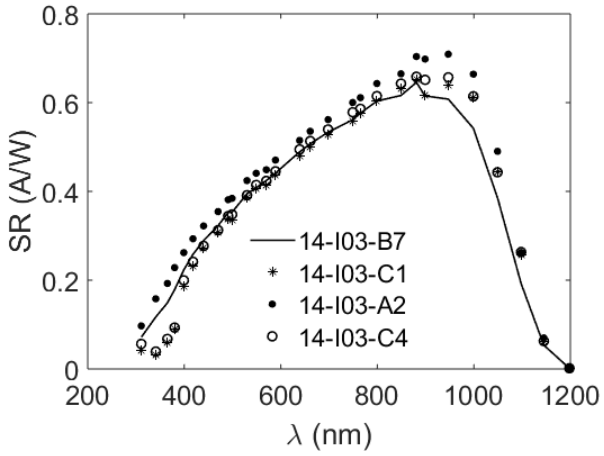

Figure 14: Comparison of spectral response curves of the crystalline reference modules: 14-I03-B7, 14-I03-C1, 14-I03-A2 and 14-I03-C4.

Figure 14 displays a strong conversion efficiency loss over the full visible spectrum of terracotta module C13-F1, with prism-shaped textured glass on the front side, with respect to the crystalline module 14-I03-B7.

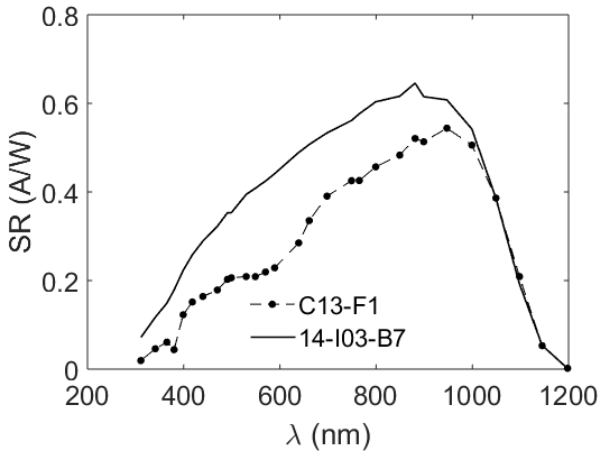

Figure 15: SR comparison between the reference module 14-I03-B7 and terracotta module C13-F1 with prism-shaped textured glass on the front side.

Similar losses are also present in figure 15 with the cantonal flag modules C13-A1 and C13-B1 with respect to the same reference crystalline module, where the impact over the short-circuit current depends on the color combination and design pattern. In this case the Appenzeller, C13-B1 takes better advantage from the blue, green and yellow spectral regions than the Glarus module C13-A1.

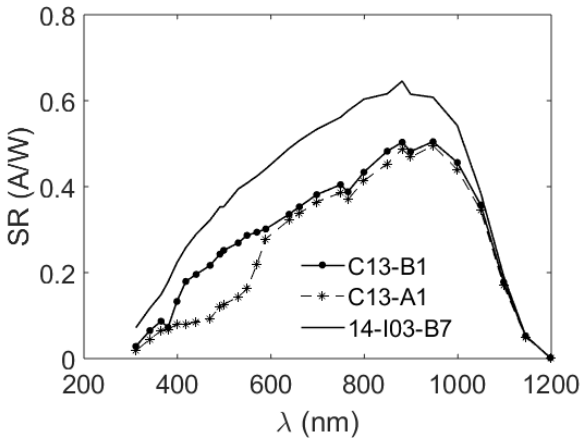

Figure 16: SR comparison between the reference module 14-I03-B7 and the cantonal flag modules C13-A1 and C13-B1 with ceramic digital printing technology.

Figure 16 compares the white module C13-D1 with its reference C13-E1. This time, the white selective filter in the front glass represents a relative loss in photo-generated current of ε_{Jsc}= 11.9% with respect to the Appenzeller flag C13-B1based on ceramic digital printing technology with white-type background.

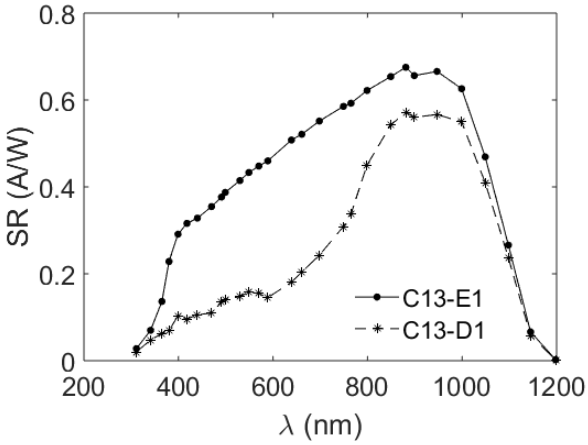

Figure 17: SR comparison between the white module C13-D1 with selective filter in the front glass and the reference C13-E1 provided by the manufacturer.

Figure 17, compares the photo-generated current of the semi-transparent terracotta module C13-I1 with respect to its reference C13-H1. This technology displays a slight decrease in performance in the blue, green and yellow spectral regions compare to the also terracotta C13-F1 with prism-shaped textured glass or the Glarus flag C13-B1 with ceramic digital printing technology with red-type background.

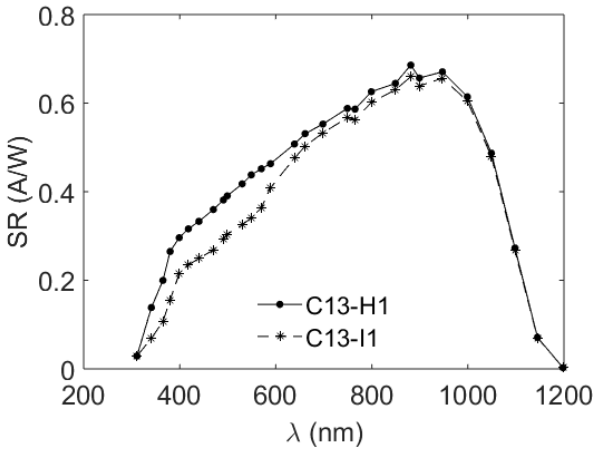

Figure 18: SR comparison between the semi-transparent terracotta module C13-I1 with mineral coating technique on glass at very high temperatures and the reference C13-H1 provided by the manufacturer.

The spectral responses of the light grey module C13-SC2 and its reference C13-SA2 provided by the same manufacturer are displayed in figure 18. Module C1-SC2 has approximately uniform losses respect to the reference C13-SA2 over the entire range of the visible spectrum.

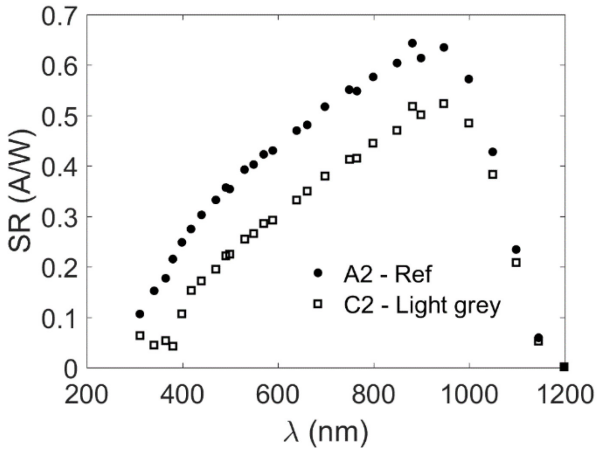

Figure 19: SR comparison between light grey module C13-SC2 and the reference C13-SA2 provided by the manufacturer.

The spectral mismatch correction in bifacial PV modules shall be applied to the front and rear measurements unless it is known that the front and rear of the bifacial device have identical spectral responsivity. The spectral responses in figure 19 show that the obtained results in the front side of the 16-074-A2 module are slightly higher than in the rear, being compatible with the bi-faciality factors found. The shape is remaining almost the same.

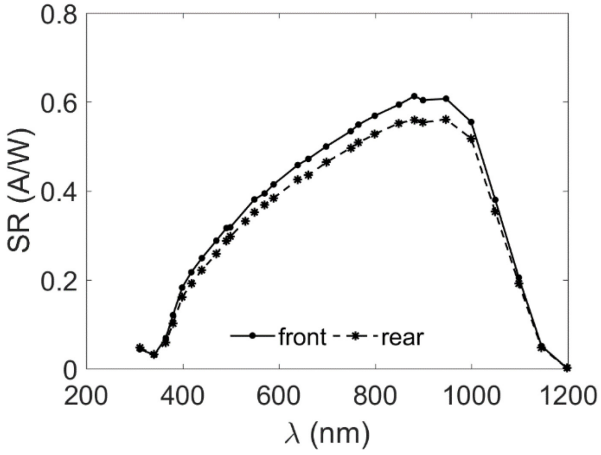

Figure 20: Comparison between the front and rear spectral responses of bifacial module 16-074-A2.

Figure 20 compares the spectral responses of the front side of the tested bifacial modules. As commented before, the modules are provided by the same manufacturer and the measurements are quite similar, just module 16-113-A1 shows a slightly higher photo-generation of charge carriers around the peak of maximum response.

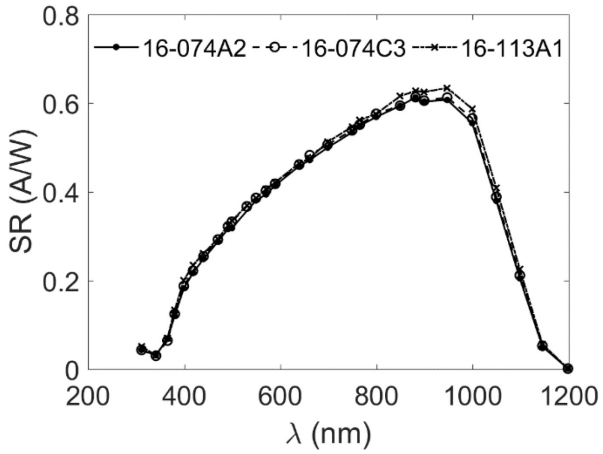

Figure 21: Comparison between the front spectral responses of bifacial modules 16-074-A2, 16-074-C3 and 16-113-A1.

Similar behavior is also found in the rear of the module. This time, the difference in photo-generation of module 16-113-A1 is also observable in the visible spectral range and consistent with the higher bi-faciality factor of this module.

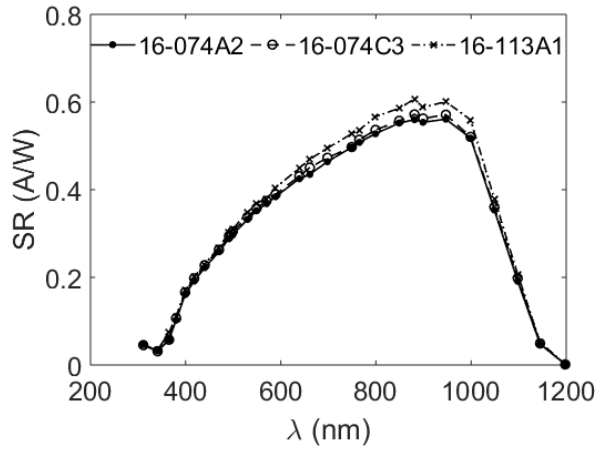

Figure 22: Comparison between the rear spectral responses of bifacial modules 16-074-A2, 16-074-C3 and 16-113-A1.

Table 6 lists the main relevant features of the performance at standard test conditions of all the photo-voltaic modules measured prior to real outdoor measurement, including the mismatch factor.
Please note that the results of the electrical characterization of bi-facial PV modules are provided, as described in the draft IEC 60904-1-2, at the equivalent irradiance levels corresponding to $G_{R_1} = 100W/m^2$ and $G_{R_2} = 200W/m^2$ and therefore the stated mismatch factor is in fact the ratio between the rear and the front one.

Label	J_{sc} (mA/cm^2)	MMF	$V_{oc}(mV)$	$FF(\%)$	$\eta_{cell}(\%)$
14-I03-B7	37.1	0.996	624.5	75.3	16.9
14-I03-C1	38.1	0.988	730.8	76.7	20.5
14-I03-A2	41.0	0.992	725.6	79.5	22.8
C13-E1	39.3	0.999	662.1	75.6	19.6
C13-D1	21.4	0.966	644.4	78.1	10.4
C13-C1	29.6	0.988	712.0	67.0	14.1
C13-C2	29.8	0.988	719.9	70.7	15.2
C13-B1	24.3	0.993	617.7	78.6	11.7
C13-A1	23.3	0.976	615.4	79.5	11.1
C13-F1	24.9	0.977	645.3	77.2	12.1
C13-H1	39.3	1.001	659.6	74.6	19.3
C13-I1	34.6	0.991	647.6	75.2	16.6
C13 – SA2	36.3	0.999	654.8	75.8	18.0
C13 – SC2	26.2	0.986	644.3	77.5	13.1
16-074-A2 (G_E =STC)	35.7	0.995	733.2	74.2	19.5
16-074-A2 (G_E =1091)	39.0	0.995	735.7	74.0	21.1
16-074-A2 (G_E =1182)	42.1	0.995	738.1	73.6	22.8
16-074-C3 (G_E =STC)	35.7	0.995	734.2	74.3	19.5
16-074-C3 (G_E =1092)	38.9	0.995	736.5	74.1	21.3
16-074-C3 (G_E =1183)	42. 2	0.995	737.0	73.9	22.9
16-113-A1 (G_E =STC)	36.1	0.994	727.1	75.8	19.9
16-113-A1 (G_E =1094)	39.5	0.994	729.9	75.3	21.7
16-113-A1 (G_E =1188)	42.9	0.994	731.8	75.0	23.5
14-I03-C4	37.8	0.993	730.8	77.0	20.4

Table 5: Characteristic parameters of the JV curves initially measured at STC

2.1.1.3. Thermal coefficients

Temperature coefficients for PV devices are commonly used for short-circuit current, α, open-circuit voltage, β, and peak power, δ. These parameters, in this work, are determined from measurements in simulated sunlight at the irradiance level of 1000W/m2. The procedure for determining the thermal coefficients is described in the international standard IEC 60891 and synthetized in figure 22, where the inset graph (a) displays the J-V curves measured each 5°C in the temperature range from 25°C to 60°C, and (b), (c) and (d) show the temperature dependence and linear regression of J_{sc}, V_{oc} and P_{mpp}.

Table 7 lists the temperature coefficients α, β and γ of the tested PV modules. Please note that the high efficiency modules 14-I03-C1, 14-I03-A2 and 14-I03-C4 and bi-facial modules considerable loss less power than the other PV modules. The modules C13-C1 and C13-C2 have not been measured up to now because of the increased measurement effort required for these devices.

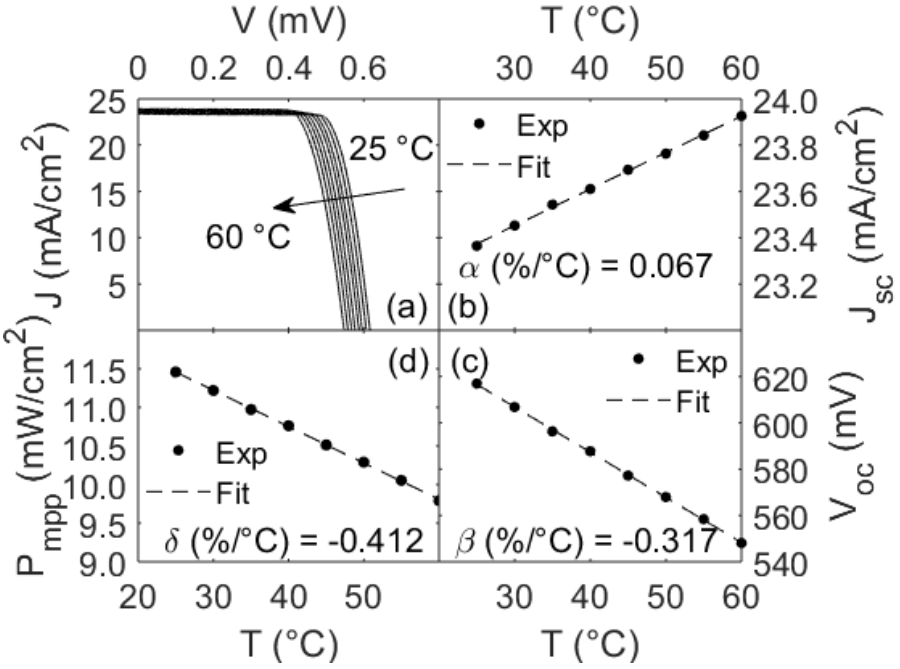

Figure 23: Determination of temperature coefficients of photovoltaic module C13-A1 at 1000 W/m2: J-V curves measured each 5°C in the temperature range from 25°C to 60°C (a) and temperature dependence and linear regression of J_{sc} (b), V_{oc} (c) and P_{mpp} (d).

Label	$\alpha(\%/K)$	$\beta(\%/K)$	$\delta(\%/K)$
14-I03-B7	0.0526	-0.3153	-0.4115
14-I03-C1	0.0506	-0.2391	-0.2640
14-I03-A2	0.0443	-0.2406	-0.2858
C13-E1	0.0487	-0.2848	-0.4031
C13-D1	0.0618	-0.3003	-0.3759
C13-C1	---	---	---
C13-C2	---	---	---
C13-B1	0.0615	-0.3159	-0.4131
C13-A1	0.0653	-0.3163	-0.4040
C13-F1	0.0450	-0.2988	-0.4288
C13-H1	0.0573	-0.2921	-0.4183
C13-I1	0.0425	-0.2992	-0.4293
C13 – SA2	0.0583	-0.2876	-0.3939
C13 – SC2	0.0463	-0.2998	-0.3995
16-074-A2	0.0435	-0.2444	-0.2773
16-074-C3	0.0435	-0.2444	-0.2773
16-113-A1	0.0470	-0.2392	-0.2554
14-I03-C4	0.0506	-0.2391	-0.2640

Table 6: Temperature coefficients for the short-circuit current (α) open-circuit voltage (β) and peak power (δ) measured according to the international standard IEC 60891

2.1.2 Inter-comparison of testing approaches for bi-facial modules

The testing protocol has been already established for the participants of the first proficiency testing on the electrical performance of bi-facial modules at the standard test conditions, as set in the draft of IEC 60904-1-2. The primary aim of proficiency testing is to help the participants to monitor the reliability of their test results, taking corrective actions where needed to improve the quality of results. This is particularly effective for ISO/IEC 17025 accredited laboratories when a new standard test procedure is released. The satisfactory results in proficiency testing may support the assessment procedure for the upgrade to the new procedure in the scope of accreditation. The results, in anonymous form, will give a direct feedback to the IEC (Technical Committee 82, Working Group 2) on the new test procedure for bifacial photovoltaic modules. The provided test items contain one mono-facial p-type PERC module, one mono-facial poly-Si module and six bi-facial modules, one module per type. Spectrally equivalent 1-cell mini-modules are also provided for participants who can measure the spectral responsivity of the samples only at cell level. Table 8 describes all the bi-facial PV modules participating in the international round robin. Supsi completed the measurement of the module on December 2018 as scheduled.

Two mono-facial modules were suppled as references for poly-Si and p-type PERC technologies and labelled as 18-i12E1 and 18-i12H1 respectively. Their current density – voltage measurement are compared in figure 23 (a), from where it is calculated that the relative performance difference between the references modules is about $\varepsilon_\eta = -10.4\%$. Figures 23 (b) and (c) compare the JV curve of the reference mono-facial module against the front and rear JV curves of poly-Si (with label 18-i12D1) and the HTJ (with label 18-i12F1) respectively. Since module 18-i12D1 is provided by the same manufacturer as the reference 18-i12E1,

If the Si wafer is assumed to be exactly the same in the reference module 18-i12E1 and the bi-facial 18-i12D1 (both supplied by the same manufacturer), the relative performance improvement of about $\varepsilon_\eta = +6.6\%$ might therefore be associated to the lower recombination junction obtained by the passivated emitter rear poly-Si. The main cell parameters are also found to be consistent to the range of best cell results achieved in industrial bi-facial polySi cells and reported by [Stodolny 2016]: $J_{sc}(mA/cm^2) = 37.5 - 38.8$, $V_{oc}(mV) = 665 - 675$, $FF(\%) = 77.8 - 79.1$ and $\eta(\%) = 19.75 - 20.72$.

The main electrical features of the silicon heterojunction PV module 18-i12F1 are also displayed in figure 23 (c) and compared against the reference module, where the significant increase in Voc agrees with the characteristic values of the technology published in [Taguchi 2014] as an example: $J_{sc}(mA/cm^2) = 39.5$, $V_{oc}(mV) = 750$, $FF(\%) = 83.2$ and $\eta(\%) = 24.7$.

On industrial-size monocrystalline Si wafers, cell efficiencies between $\eta(\%) = 19.0$ with $J_{sc}(mA/cm^2) = 37.9$, $V_{oc}(mV) = 635$, $FF(\%) = 79.0$ and between $\eta(\%) = 20.2$ with $J_{sc}(mA/cm^2) = 38.9$, $V_{oc}(mV) = 652.0$, $FF(\%) = 79.9$ have been obtained by different groups such as Münzer 2011 and Engelhart 2011 respectively. The JV curve of our p-type PERC mono-facial reference module is compared in figures 23 (d), (e) and (f) against the front and rear JV curves of the bi-facial p-type PERC with labels 18-i12G1 and 18-i12C1 from the same manufacturer and the n-type PERT bi-facial modules 18-i12A1 and 18-i12B1 from other manufacturers. The efficiency of our reference module remains $\eta(\%) = 20.2$ as in Engelhart 2011, but an increase of roughly $0.5\ mA/cm^2$ in short-circuit current and $10\ mV$ in open-circuit voltage that compensate the $2.4\ \%$ loss in fill factor, suggest that there are significant differences between both p-PERC concepts.

The mono-facial module 18-i12H1 is compared against the bi-facials 18-i12G1 and 18-i12C1 of the same manufacturer in figure 24 (d). Module 18-i12G1 is a 60-cells module connected in series and its main electrical features are quite similar to the reference module 18-i12H1. However, module 18-i12C1 is assembled with two strings in parallel with 72-half cells connected in series and shows an increase of $20\ mV$ in open-circuit voltage with respect to the reference module. The differences in layout does not explain the increase in the normalized open-circuit voltage[1] and it might suggest differences in the carrier lifetime due possible variations in the process sequence of passivation.

[1] Please note that the short-circuit currents and open-circuit voltages have been normalized to the value of a single equivalent cell of one square centimeter by means of the area and number of the cells in each module for the sake of comparison between different modules.

The comparison between the mono-facial reference p-type PERC 18-i12H1 and bi-facial n-type PERT modules 18-i12B1 and 18-i12A1 is displayed in figures 23 (e) and (f) respectively. Module 18-i12B1 is also assembled with two strings in parallel but with 60-half cells connected in series and module 18-i12A1 is a standard 60-cell module. The short-circuit current from module 18-i12B1 and 18-i12A1 remains similar to the reference, but the open-circuit voltage in 18-i12B1 and 18-i12A1 is roughly $12\ mV$ lower and $11\ mV$ higher respectively than the reference module 18-i12H1.

Module Reference	**Label**	**Cell Technology**	**Remark**
LR6-60PE-A1	18-i12H1	p-type PERC	Manufacturer 1: mono-facial reference module
JKM270PP-A1	18-i12E1	poly-Si	Manufacturer2: mono-facial reference module
LR6-60BP-A1	18-i12G1	p-type PERC	Manufacturer 1: 60 cells
JKM300-60-A1	18-i12A1	n-type PERT	Manufacturer 2: 60 cells
JHNM60-A1	18-i12F1	HJT	Manufacturer 3: 60 cells
LYGF-QP60TPG-A1	18-i12B1	n-type PERT	Manufacturer 4: 120 cells
LR6-72BP-A1	18-i12C1	p-type PERC	Manufacturer 1: 72 cells
CS3U-350PB-A1	18-i12D1	poly-Si	Manufacturer 5: 144 cells

Table 7: List of PV modules participating in the international round robin

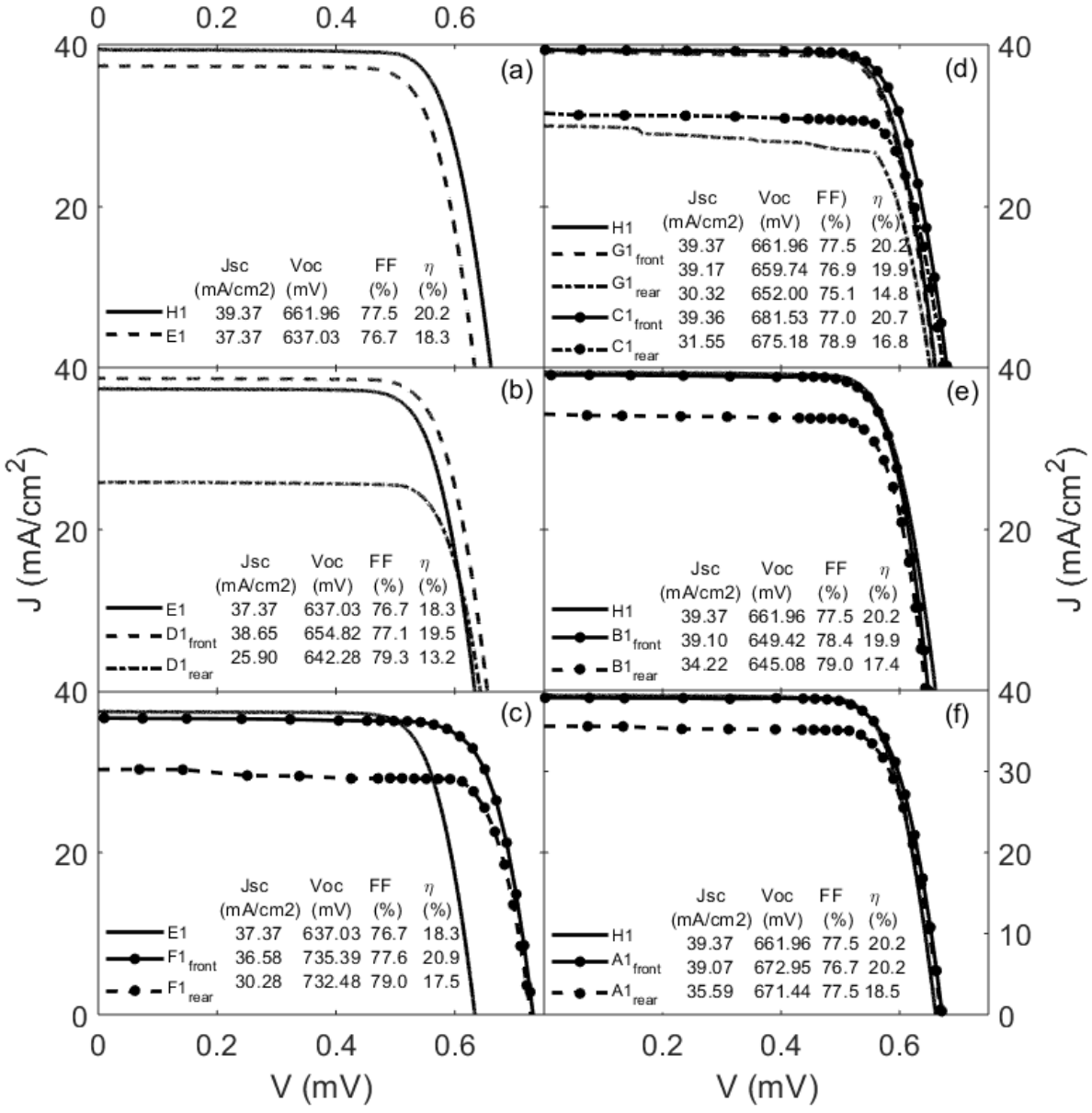

Figure 24: Comparison of current density – voltage, JV, curves of PV modules participating in the international round robin: (a) poly-Si and p-type PERC mono-facial references labelled as 18-i12E1 and 18-i12H1 respectively. Reference 18-i12E1 against the front and rear performance of the bi-facial (b) poly-Si module with label 18-i12D1 and (c) HTJ module with label 18-i12F1. The mono-facial module 18-i12H1 is compared against the front and rear performance of the bi-facial (d) p-type PERC modules 18-i12G1 and 18-i12C1 of the same manufacturer and n-type PERT modules with labels (e) 18-i12B1 and (f) 18-i12A1.

The front and rear power generation of the module 18-i12G1 as a function of the front equivalent and rear irradiance is displayed in figure 24. Although the rate of change in the maximum power as the irradiance change are similar, other cases like 18-i-12C1 in figure 25 shows a significant change of trend that reveals a small reduction of the generated power in the high illumination regime, above one sun. It

is important to note that while module18-i12G1 is a 60-cells serially connected, module 18-i12C1 is a 72-cells serially connected. Although no significant differences were appreciated between their fill factor in figure 24 at standard test conditions, the overall series resistor might be higher in module 18-i12C1 and therefore limits the generated power.

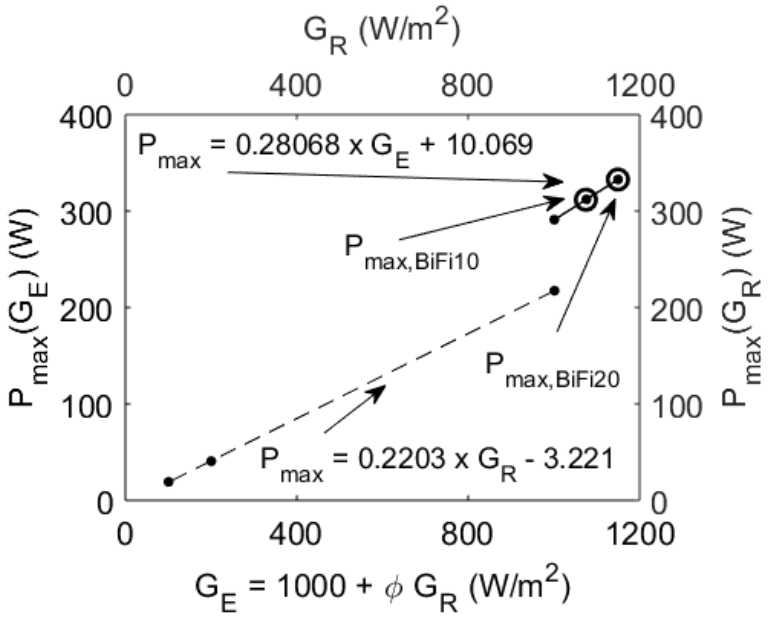

Figure 25: Rate of change in front and rear maximum power as the front equivalent and rear irradiances change in module 18-i12G1.

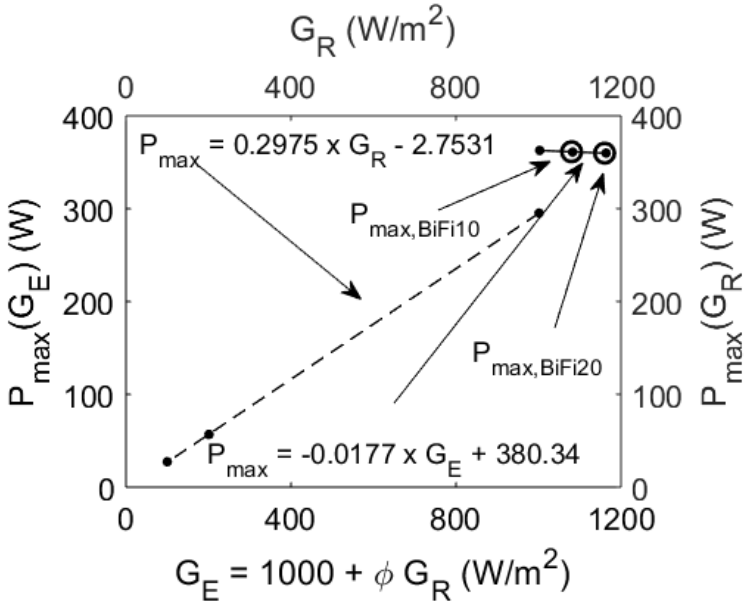

Figure 26: Rate of change in front and rear maximum power as the front equivalent and rear irradiances change in module 18-i12C1.

The list of measurands requested by the international proficiency test of bi-facial modules and measurement results at Supsi are listed in table 9. However, the evaluation and results of the proficiency testing is not available at the moment of writing this final project report and it will be communicated later throughout international conferences.

Mesurand	Irradiance [W/m^2]		18-i12G1	18-i12C1	18-i12A1	18-i12F1	18-i12B1	18-i12D1
I_{sc}^{STC} front	1000	A	9.518	9.558	9.473	8.882	9.474	9.412
V_{oc}^{STC} front	1000	V	39.585	49.070	40.377	44.123	38.965	47.147
P_{max}^{STC} front	1000	W	290.983	362.686	295.471	305.879	291.435	343.622
I_{sc}^{STC} rear	1000	A	7.355	7.649	8.611	7.341	8.3137	6.2980
V_{oc}^{STC} rear	1000	V	39.1198	48.613	40.286	43.949	38.705	46.245
P_{max}^{STC} rear	1000	W	217.425	295.203	271.296	256.675	255.468	232.019
φ_{Isc}		-	0.7728	0.8002	0.9090	0.8265	0.8775	0.6691
φ_{Voc}		-	0.9882	0.9907	0.9977	0.9961	0.9933	0.9809
φ_{Pmax}		-	0.7472	0.8139	0.9182	0.8391	0.8766	0.6752
φ		-	0.7472	0.8002	0.9090	0.8265	0.8766	0.6691
I_{sc} rear	100	A	0.728	0.777	0.866	0.7408	0.8384	0.6258
V_{oc} rear	100	V	35.114	45.492	36.401	39.679	35.193	41.036
P_{max} rear	100	W	19.242	27.372	25.700	23.490	23.575	20.691
I_{sc} rear	200	A	1.458	1.545	1.727	1.474	1.671	1.260
V_{oc} rear	200	V	36.312	45.969	37.304	40.293	35.918	42.643
P_{max} rear	200	W	40.638	56.811	52.930	48.782	48.851	43.457
I_{sc} front	$G_E = 1000 + 100\varphi$	A	10.2327	9.555	9.470	8.900	9.456	10.0327
V_{oc} front	$G_E = 1000 + 100\varphi$	V	39.712	49.134	40.531	44.203	39.097	47.195
P_{max} front	$G_E = 1000 + 100\varphi$	W	312.186	360.980	294.065	305.653	291.769	365.025
I_{sc} front	$G_E = 1000 + 200\varphi$	A	10.929	9.560	9.468	8.884	9.460	10.665
V_{oc} front	$G_E = 1000 + 200\varphi$	V	39.812	49.284	40.636	44.310	39.228	47.336
P_{max} front	$G_E = 1000 + 200\varphi$	W	332.747	359.839	292.715	305.172	291.404	388.082
MMF front		-	0.9953	0.9953	0.9930	0.9944	0.9929	0.9961
MMF rear		-	0.9937	0.9937	0.9909	0.9930	0.9957	0.9949
Slope		m^2	0.2203	0.2975	0.2723	0.2586	0.2574	0.2348
P_{max} vs G_R								

Table 8: List of measurands requested in the international proficiency test of bi-facial modules and measurement results at Supsi.

2.2 Outdoor performance and modelling

Background:
The performance evaluation of PV modules requires outdoor testing in order to compare the energy yield of different technologies. The instantaneous power, current-voltage characterization and module temperature have therefore to be monitored under real operating conditions, and the stability controlled. This is of particular interest for all commercial technologies, for which nearly no detailed outdoor data are available or for the new generation technologies, that claim better performance and innovative solutions.
Regarding the specific case of bifacial modules, in order to have all the relevant data to achieve a correct performance prediction and module labelling, and to link it to an accurate and reproducible bifacial PV plant simulation, it is important to develop an innovative and focused “bifacial test facility” to collect all the relevant module parameters and all the relevant meteorological parameters

Scope of the project:

- Refurbishment of the existing outdoor test facility.
- Set-up of a dedicated outdoor test stand for bifacial modules.
- Performance analysis under real operating conditions of new technologies and evaluation of the impact of special features or the use of new materials on the performance.
- Propose new labelling solutions for more innovative technologies (e.g bifacial or BIPV modules)

Results:

- The outdoor test facility at SUPSI has been refurbished. Calibrations and/or replacements of hardware have been performed in order to keep the testing equipment updated and to fulfil the requirements of the recommendations given in the best practice guideline reported in IEA-PVPS T13-11:2018 .
- A new website has been designed and set-up for the publication and monitoring of outdoor data from different PV infrastructures. The main concept is based on site-specific dashboards that help to ensure accurate operation and standardized performance indicators through constant, solid and traceable monitoring environment.
- One year of outdoor measurement of aesthetics modules have been successfully concluded and the performance of the colored modues have been compared respect to their reference modules.
- Depending on the colour technology (type and uniformity of color/s and level of cell camouflage) yield differences respect to the reference modules of 16-45% have been observed in the field. The differences are the sum of losses or gains which can be estimated from the module parameters measured in the laboratory and presented in chapter 2.1.
- Good match of calculated to measured yields could be demonstrated for clear sky conditions.
- It was demonstrated that the STC power loss explains most of the performance differences observed in the field, but it is not sufficient for a fair inter-comparison of colored modules. Thermal, spectral and angular effects have to be taken into account stressing the need of a full characterisation according 61853 part 1 and part 2.
- In particular, the temperature of the modules is strongly affected by the colour coating. A decrease of up to 10ºC was observed for the white module when mounted in Lugano at 45º and open-rack conditions. The same effect, but in a minor extend was observed for the light grey (silver) module.
- As known for thin film technologies, the spectral effect has to be considered when simulating the outdoor performance of colored modules.

- As demonstrated with the textile module, the use of bifacial cells can help to partially compensate the performance losses caused by the aesthetical changes.
- The non-uniformity of irradiance in the rear of bi-facial modules has been analysed in more detail. It depends on the surroundings of the module and day number of the year, being at our test site lower than 10% (as required by the new standard IEC 60904-1-2 for the outdoor power generation gain measurement) under clear sky conditions.
- The median of the temperature's non uniformity depends also on the surroundings of the module and day number of the year, being found to be in general below 5%.
- The three tested bi-facial modules clearly outperformed the crystalline reference module over the analysed clear sky days with daily relative differences in energy yield between 8% and 12% (depending on the clear sky day) when using the rated front power measured indoor at standard test condition. If bi-facial modules were commercially priced as an equivalent peak power of P_{GE10}, the boosted energy would have been drastically reduced up to a maximum of 1.2%. If the bi-facial modules had been marked as P_{GE20}, they would have underperformed around -7%.
- White and black diffuse reflectors were investigated for its applications in the built environment, where the rear panels might act as rooftops or wall surfaces. They increase the non-uniformities in irradiance with respect to the configuration without any reflector on the rear of the modules, and reach instant values considerable higher than 10%. The non-uniformities in temperature remains generally below 5%.
- Daily relative differences of performance between bi-facial modules with white reflectors and the crystalline reference are in general above 20%. Within this mounting conditions, if the bi-facial module were commercially rated as $PGE10$ or $PGE20$, it still outperforms the reference crystalline with relative differences above +10% and +3% for $GE10$ and $GE20$ respectively.
- Bi-facial modules with black rear reflectors still outperform the mono-facial reference below 5% when rated at standard test conditions. However, it would underperform if they were commercially rated either as $PGE10$ or $E20$.

2.2.1 Refurbishment of outdoor test facility

The mounting structure and surrounding of the test facility for the outdoor performance assessment of PV modules at SUPSI was chosen to maximize the availability of data (minimizing possible rejections by reflections or shading effects from nearby objects like buildings, trees or fences, for example) and uncertainty of the sum of energy delivered. The mounting configuration is an open-rack configuration, tilted and oriented closely to the optimum at the geographical location for the modules to receive the highest yearly insolation.

The layout of the test racks in figure 26 for aesthetic and 27 for bi-facial modules has been designed considering the best practice guidelines reported in IEA-PVPS T13-11:2018. It guarantees a coplanar installation of the test modules and irradiance sensors so that all modules and sensors have the same tilt and orientation angle. The heights of the test samples have been defined at least one meter above the ground and 10 centimeters from any other object in order to promote the air circulation around the modules and minimize temperature gradients. Additional dummy modules on the left and right of the row have been placed in order to reduce the heat propagation by convection mechanism in these module locations.

The hardware solutions used for the measurement of the module power combines IV-tracing (IV) performed in regular intervals while the module is otherwise operated at its maximum power by means of maximum power point trackers (MPPT). New hardware components have replaced the old ones and full calibration campaign on the installed all-in-one instruments has been conducted before the installation. The available hardware solutions with the connected sensors and calibrated loads are listed in table 10.

A deep understanding of the module performance and stability requires information about environmental parameters like in-plane irradiance, module temperature and spectral irradiance. For further analysis, our test facility is also equipped with sensors for the measurement of ambient temperature, wind condition relative humidity and precipitation.

The spectral irradiance at SUPSI is scanned with an array detector spectroradiometer yearly checked within the international spectroradiometer intercomparison campaign that the European Solar Test Installation, ESTI, organize together with the top European research laboratories in different parts of the world for comparing primary instruments for spectral solar irradiance measurements and broadband radiation sensors. The calibrated sensitivities of the in-plane global broadband detectors used in the test benches are listed in table 11 and the assemblies of the test racks for the outdoor assessment of aesthetics and bi-facial PV modules are shown in figures 28 and 29.

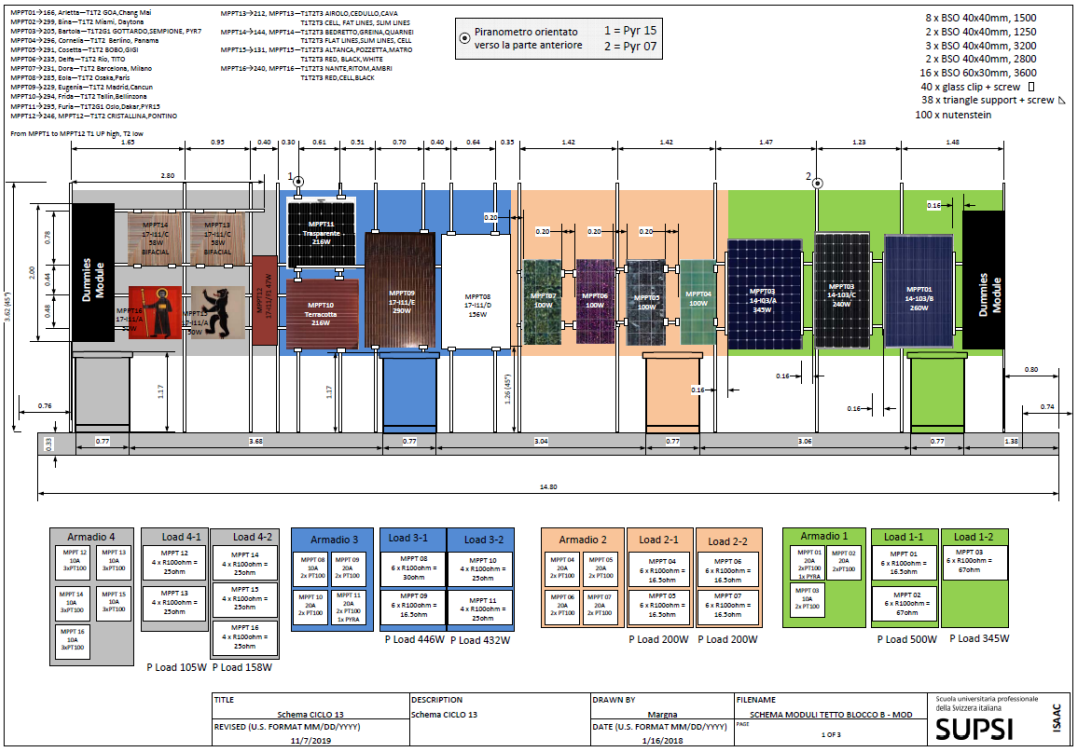

Figure 27: Layout design of the test rack for aesthetic modules

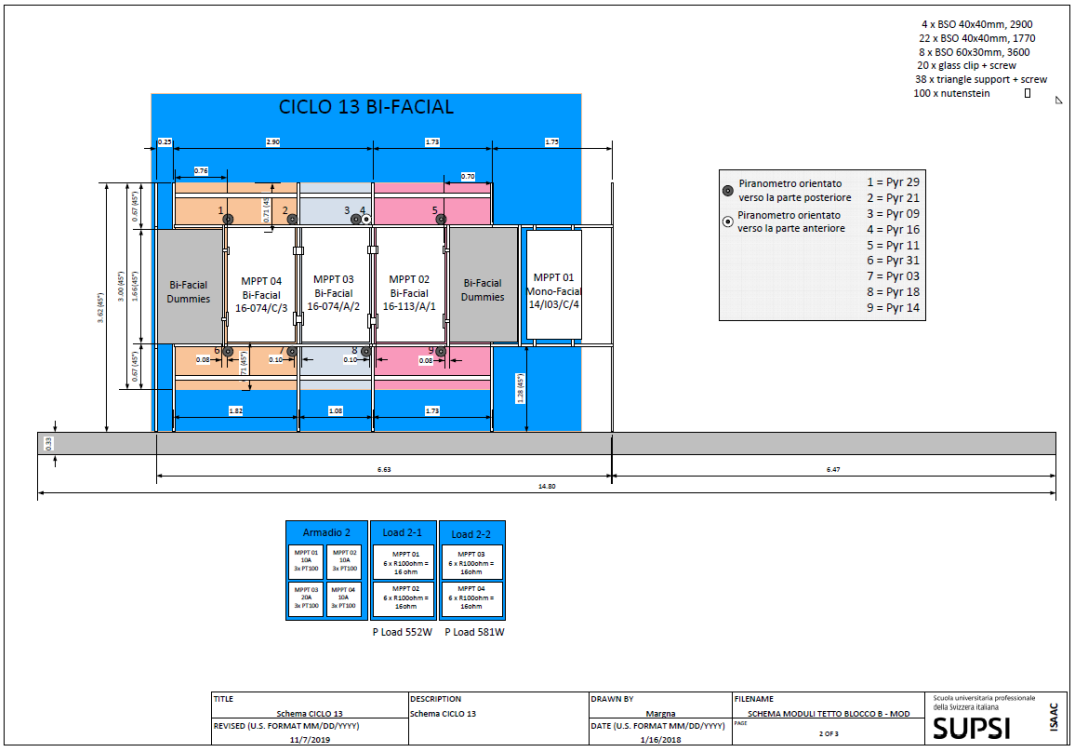

Figure 28: Layout design of the test rack for bi-facial modules

Module	Hardware	Max. Current (A)	Sensors	Load (Ohm)
14-I03-B7	MPPT1	20	2xPT100	16.5
14-I03-C1	MPPT2	20	2xPT100	67.0
14-I03-A2	MPPT3	10	2xPT100	67.0
C13-E1	MPPT9	20	2xPT100	16.5
C13-D1	MPPT8	10	2xPT100	30.0
C13-C1	MPPT13	10	3xPT100	25.0
C13-C2	MPPT14	10	3xPT100	25.0
C13-B1	MPPT15	10	3xPT100	25.0
C13-A1	MPPT16	10	3xPT100	25.0
C13-F1	MPPT12	10	3xPT100	25.0
C13-H1	MPPT12	20	2xPT100	25.0
C13-I1	MPPT10	20	2xPT100	25.0
C13 – SA2			2xPT100	
C13 – SC2			2xPT100	
16-074-A2	MPPT3B	20	3xPT100	16.0
16-074-C3	MPPT4B	10	3xPT100	16.0
16-113-A1	MPPT2B	10	3xPT100	16.0
14-I03-C4	MPPT1B	10	3xPT100	16.0

Table 9: List of all-in-one hardware solution for the measurement of PV module power and calibration values

Pyranometer	Location	Model	Sensitivity $(\mu V/W \cdot m^2)$	Uncertainty (%)
PYR07	Aesthetics	CMP11	8.771	1.56
PYR15	Aesthetics	CMP11		
PYR21	BiFi front	CMP11	5.192	1.46
PYR31	BiFi back	CM11	4.813	1.45
PYR14	BiFi back	CM11	4.803	1.39
PYR03	BiFi back	CM11	4.640	1.52
PYR11	BiFi back	CM11	5.537	1.44
PYR09	BiFi back	CM10	5.488	1.55
PYR16	BiFi back	CM11	4.922	1.50
PYR29	BiFi back	CM10	4.422	1.49
PYR18	BiFi back	CM10	5.470	1.72

Table 10: List of broadband detectors and calibrated sensitivities.

Figure 29: Picture of the test stand for aesthetic moduless

Figure 30: Picture of the test stand for bi-facial modules

2.2.2 Webpage for the publication of outdoor data

A new website has been designed and set-up for the publication and monitoring of outdoor data from different PV infrastructures. The main concept is based on site-specific dashboards that help us to ensure accurate operation and standardized performance indicators through constant, solid and traceable monitoring environment.
The architecture is designed to collect data from multiple sources, store them in InfluxDB, and display graphs and statistics in an efficient way, please see figure 30. InfluxDB is a time-series database which has experienced an exponential growth in recent years, with the popularization of internet of things IoT, big data and other technologies that collect a lot of information over time. It efficiently manages these data series, with thousands of data per second, allowing analysis of myriads of data in real time. The open source platform Grafana, beautifully checks and visualizes data series for the analysis of PV infrastructures. It is a very powerful tool with an elaborated query editor, which allows choosing among previously defined metrics and performing data treatment and analysis. This tool supports a system alert that can be easily configured to prevent mal-functioning, data rejection or any other circumstance. Access to data remains under restricted use due to confidentiality agreements. However, future projects could be oriented to public domain.

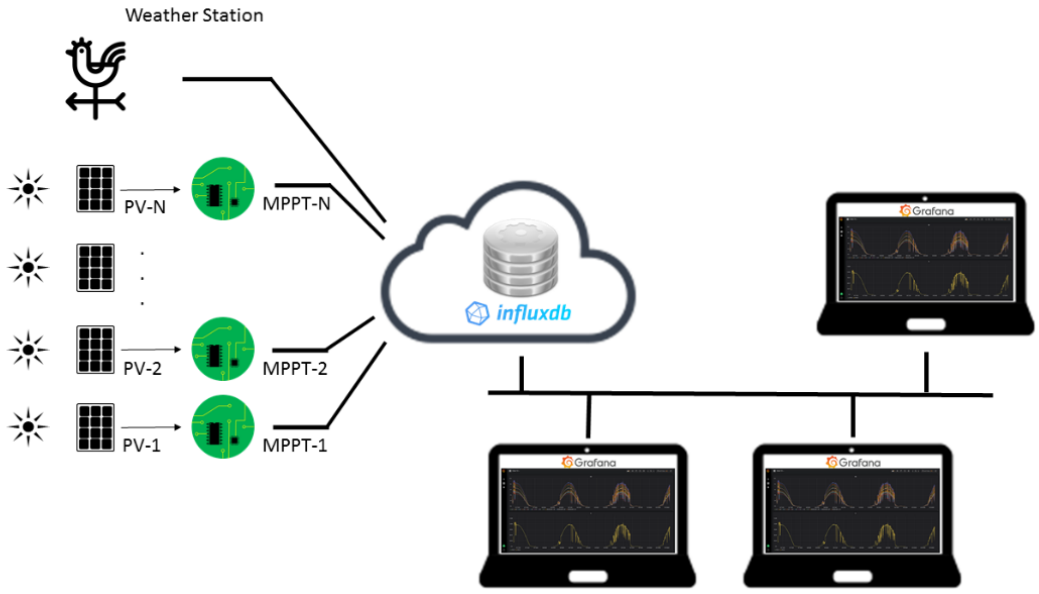

Figure 31: IT architecture for outdoor performance assessment of photovoltaic modules

2.2.3 Analysis of results and discussions

2.2.3.1. Aesthetic modules

kWh Measurements and inter-comparison

The loss in energy yield caused be different colour treatments or other changes in aesthetics depends on many factors. To better understand the performance under real operating conditions, the coloured modules have been monitored for an entire year (starting from 1 May 2018) together with its reference modules and the difference in kWh respect to these was calculated. In the optimal case a module of the same type (same cells, interconnection and module manufacturing), but without colour treatment was available. In this case a direct inter-comparison was possible. If not, a commercial module with the same cell technology and similar cell efficiency had to used instead.

Table 12 and Figure 31 shows the results of the 1year kWh inter-comparison once normalized to the active area (cells in series*cell area) and once to the indoor measured STC power. 1 module per type was here analysed. The 2 modules C13-SA2 and C13-SC2 were delivered later in the project and data are so limited to approx. 4 month of data.

Test modules	**SUPSI Lable**	**(a) 1 YEAR**		**(b) 1 YEAR (clear days)**	
		ΔkWh/m²	**ΔkWh/W**	**ΔkWh/m²**	**ΔkWh/W**
REF	C13-E1				
white	C13-D1	-44.5%	4.8%	-43.1%	7.4%
REF	C13-H1				
terracotta	C13-I1	-16.0%	-4.4%	-16.5%	-4.2%
REF	C13-SA2				
light grey/silver	C13-SC2	-28.3%	-0.1%	-27.7%	1.0%
REF HJT	14-I03-C1				
textile/bifacial	C13-C2	-23.8%	9.5%	-26.0%	7.0%
red facade	C13-F1	-45.1%	-5.3%	-46.4%	-6.3%
REF poly	14-I03-B7				
Appenzell	C13-B1	-34.3%	-3.9%	-34.8%	-3.8%
Glarus	C13-A1	-38.8%	-5.5%	-38.5%	-5.1%

Table 11: Annual kWh inter-comparison between coloured and transparent modules normalized to the module active area [kWh/m^2] and to the measured STC power [kWh/Wp] for all days of the year (a) and for all clear days (b).

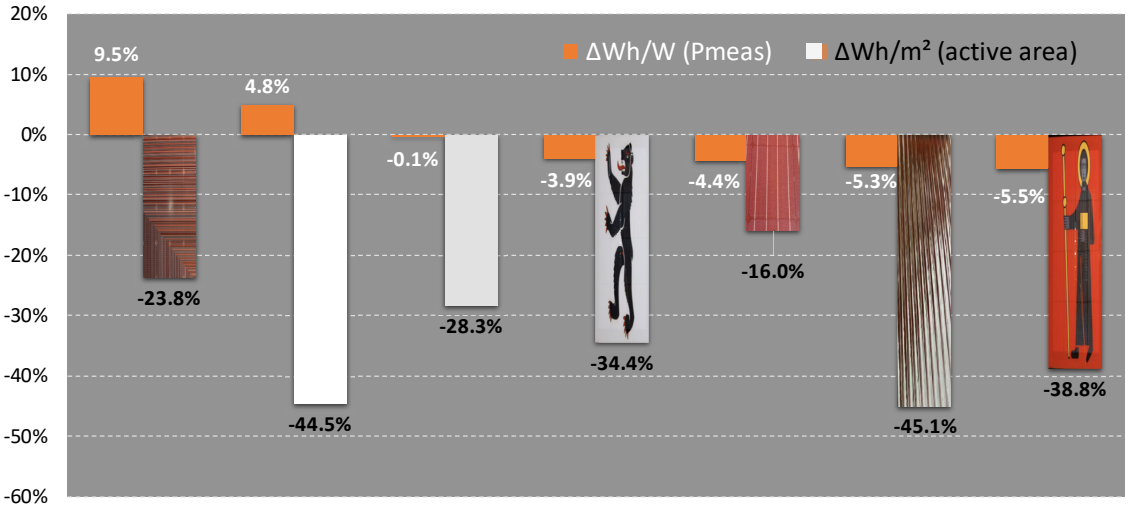

Figure 32: Annual kWh inter-comparison between coloured and transparent modules normalized to the module active area [kWh/m^2] and to the measured STC power [kWh/Wp].

The kWh/m^2 inter-comparison shows significant differences in the power density of 16 up to 45.1%, depending on the colour of the coating and its density. The yield difference is dominated by the relative cell efficiency loss measured at STC with the solar simulator. This loss is already summarised and explained in chapter 2.2.1.1 and 2.2.1.2. As expected, the losses in short circuit current and respectively in power and energy production are the highest for the modules in which the cells are completely hidden behind the coating, which are here the white and terracotta façade module with deep structured glass. The lowest difference is the one of the terracotta module, where the cells interconnects are still visible by eye.

As expected, when normalising the kWh to the measured STC power, the differences reduces significantly highlighting other effects like: module temperature reached in the field, response to daily and seasonal spectral variations, angular response or other module features like the use of bifacial cells. In some cases, this leads to a gain respect to the reference module, like for the bifacial module with textile printing which shows a gain of 9.5% respect to its reference and the white module with 4.8%. The others show a neutral or negative budget of up to -5.5%.

The example of the textile module shows how the use of bifacial cells can partially compensate the relative efficiency loss due to the colour printing. In the case of the white module the gain is to be fully attributed to the coating itself. Beside the large loss due to spectral response, the spectral selective foil used for the white module has the advantage to reflect and diffuse the visible spectrum providing a white appearance, while the infrared part is transmitted and converted into electricity. The same effect can be seen in a minor extend in the light grey module. This leads on one side to a lower operating temperature, which can be seen in Figure 32, and on the other side to a lower spectral mismatch over the day.

As shown in figure 32, the back of module temperature of the white module measured at a clear summer day is around 10 °C lower respect to the other modules, whereas in the light grey module it is around 3.5°C lower.

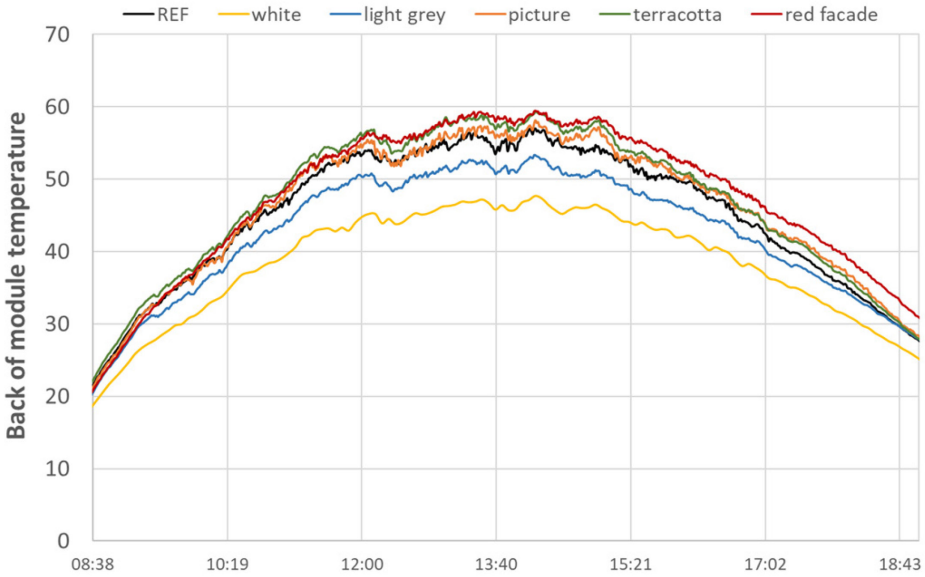

Figure 33: Example of back of module temperature of the modules under test measured during 1 day in August.

Loss Calculations (methodology)

To explain the yield differences, the single loss factors due to STC efficiency, temperature, irradiance, spectral irradiance, angle of incidence and back irradiance has to be calculated and compared to the measured value.

In a simplified approach the power output can be described by the following equations:

$$P_m = P_{stc} \cdot G_{eff}/1000 \cdot [1 + \delta \cdot (T_{\mathrm{mod}} - T_{stc})] \cdot [1 + b \cdot \ln(G_{eff}/G_{stc}) + c \cdot \ln^2(G_{eff}/G_{stc})] \quad [1]$$

$$G_{eff} = I_{sc,meas} \cdot [1 + \alpha \cdot (T_{\mathrm{mod}} - T_{stc})] \cdot \frac{G_{stc}}{I_{sc,stc}} \quad [2]$$

$$T_{\mathrm{mod}} = ECT = 25 + \frac{1}{\beta} \cdot \frac{V_{oc,meas}}{V_{oc,stc}} - 1 - a \cdot \ln(\frac{G_{eff}}{G_{stc}}) \quad [3]$$

where,

$$G_{stc} = 1000\,W/m^2 \quad , \quad T_{stc} = 25°C$$

The inputs for the equations are either measured indoors ($I_{sc,stc}$, $V_{oc,stc}$, $P_{stc,}$, α, β and δ) or are extracted from the measurement at different irradiances (a,b,c).

The performance of the device under test (P_{DUT}) can be now expressed starting from the performance of the reference device (P_{REF}):

$$P_{DUT} = P_{REF} \cdot \frac{P_{DUTstc}}{P_{REFstc}} \cdot \frac{G_{DUTeff}}{G_{REFeff}} \cdot \frac{[1 + \gamma_{DUT} \cdot (ECT_{DUT} - 25)]}{[1 + \gamma_{REF} \cdot (ECT_{REF} - 25)]} \cdot \frac{[1 + a_{DUT} \cdot \ln(G_{DUTeff}/1000) + b_{DUT} \cdot \ln^2(G_{DUTeff}/1000)]}{[1 + a_{REF} \cdot \ln(G_{REFeff}/1000) + b_{REF} \cdot \ln^2(G_{REFeff}/1000)]}$$

The specific losses L_x due to differences in STC performance, spectral mismatch, module temperature and irradiance dependency are then calculated as follow:

$$E_{DUTcalc} = E_{REFmeas} \cdot (1 + L_{stc}) \cdot (1 + L_{Isc}) \cdot (1 + L_{temp}) \cdot (1 + L_{irrad})$$

From these the total Loss L_{tot} can be calculated:

$$L_{tot} = \prod(1 + L_x) - 1$$

Following assumptions have been done for the calculations of the Losses L_{stc}, L_{Isc}, L_{temp} and L_{irrad}:

- The temperature coefficient is given by the cell technology and does not changes with the coating. The temperature coefficient measured on the transparent module was used.
- The module temperature measured on the back of the module is underestimating the cell temperature - especially for the glass/glass modules - and the equivalent cell temperature (ECT) is used instead.
- The change of angular response due to the coatings is here neglected. The separate estimation of the AOI loss will be included as soon the measurement of the AOI dependency of full modules will be finalised. The effect is here included in the Isc loss.

Example (white module)

Figure 33 shows the measured power output (Pm) of the white device under tests (DUT) and its transparent reference module (REF) for a single clear sky day. The 4 loss contributions (L_{stc}, L_{Isc}, L_{temp} and L_{irrad}) have been calculated according the procedure described before and plotted in Figure 34 and compared with the measured power of the white device under test.

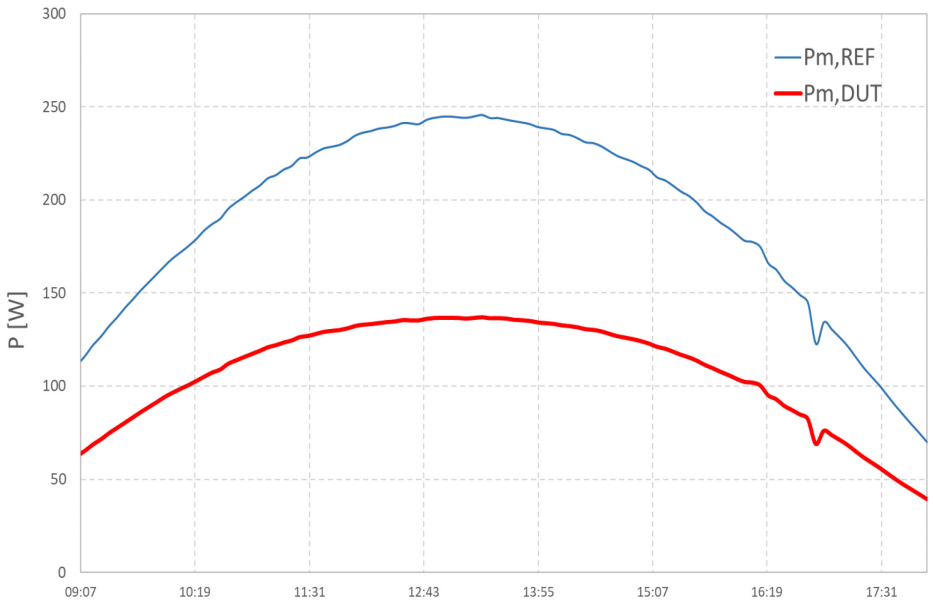

Figure 34: Measured power output of the white module and its reference module.

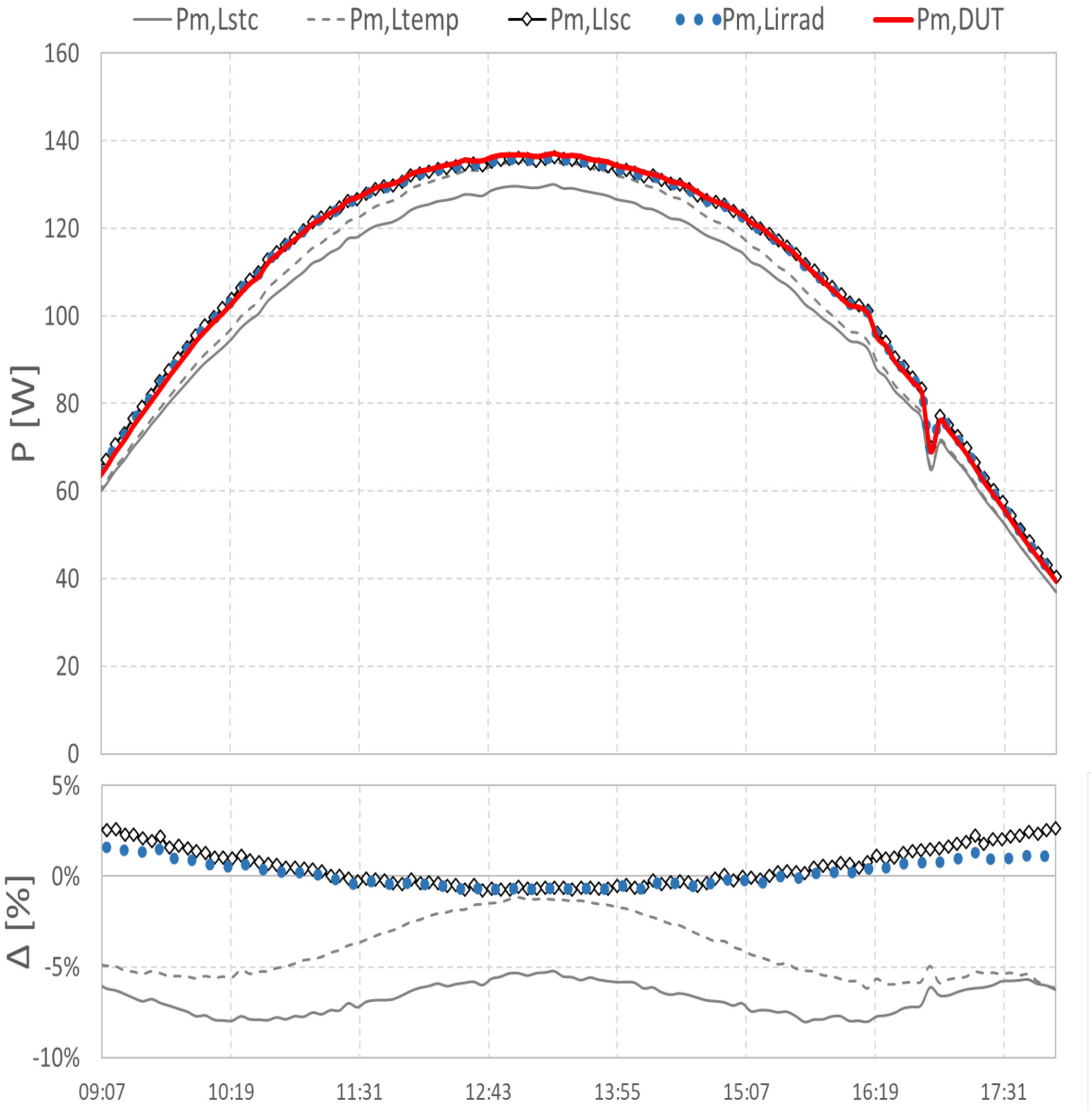

Figure 34: Calculated Pm,Lstc, Pm.LIsc, Pm.Ltemp and Pm,Lirrad versus measured power Pm,DUT (in red) for the white module measured within a single clear sky day and the respective difference between measured and calculated power (bottom figure).

The first basic correction for STC power (L_{stc}), shown as continues grey line, leads to a general underestimation of the power over the whole day (RMSE = -6.7%). By taking into account the thermal loss (L_{temp}) a major improvement at solar noon is achieved (RMSE= -3.7%), here depicted as grey interrupted line. With the subsequent correction for short circuit losses (L_{Isc}) most of the remaining deviations of the day is corrected approaching already very well the real measured power (RMSE=0.3%). The last correction for the relative efficiency loss (L_{irrad}) further improves the prediction but in a much lower extend. The final calculated power, which takes so into account all losses, depicted in figure 34 as filled blue dots, approximates very well the measured power (RMSE=0.0%, STDEV=0.7%).

Figures 35 and 36 shows the accord. [2] and [3] calculated equivalent cell temperature (ECT) and effective irradiance (G_{eff}) respect to the measured back of module temperatures (T_{bom}) and the in-plane irradiance measured with a pyranometer (G_{pyr}). The relation between the two effective irradiance values of DUT and REF determines the correction which is applied for the calculation of L_{Isc}.

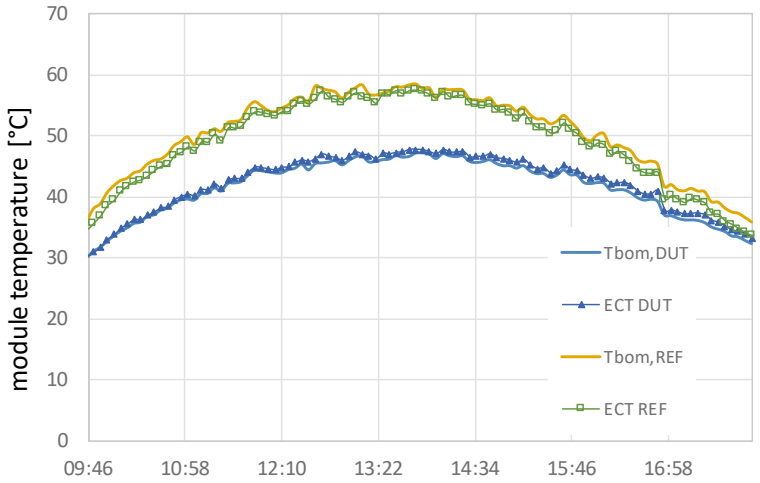

Figure 35: Measured back of module temperature (Tbom) and calculated equivalent cell temperature (ECT) for the white module (DUT) and the transparent module (REF).

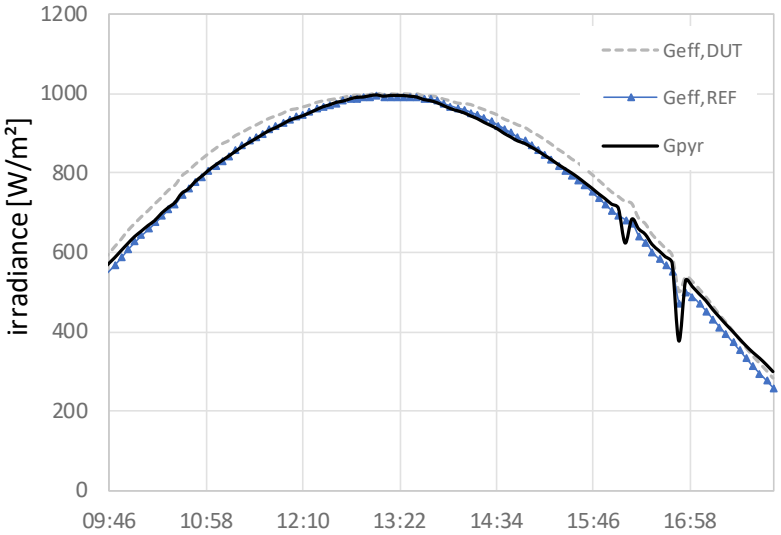

Figure 36: Global irradiance measured with a pyranometer (Gpyr) and effective irradiance (Geff) calcultaed with the measured short circuit current of the white module (DUT) and the transparent module (REF).

Loss Calculations (results)

Table 13 shows the single losses of some selected colored modules for a single clear sky day. It can be seen that the calculated loss L_{tot} corresponds very well to the measured one.

	Measured ΔkWh/m² [%]	L_{stc} [%]	L_{temp} [%]	L_{Isc} [%]	L_{irrad} [%]	L_{tot} [%]
white	-44.2	-47.1	3.3	2.2	-0.3	-44.3
silver	-26.7	-28.4	1.8	1.0	-0.2	-26.5
Appenzell	-35.9	-31.9	-0.4	-5.7	0.6	-35.6
terracotta	-16.4	-12.1	-1.8	-2.7	0.1	-16.0
red facade	-48.8	-41.7	-7.8	-4.8	0.5	-48.6

Table 12: Measured loss Loss factors (L_{stc}, L_{Isc}, L_{temp}, L_{irrd} and L_{tot}) for each module together with the.

The results allow to clearly discern the different losses L_{stc}, L_{Isc}, L_{temp} and L_{irrad}. It can be seen that in all cases, the STC loss is not sufficient to describe the outdoor performance. Of the secondary effects the major impact is given by the thermal and the I_{sc} loss. L_{Isc} is driven by the change in spectral mismatch over the day and the position of the sun. The impact due to a change in relative efficiency loss $\eta_{rel}(G)$, caused by the coatings has only a minor impact to the overall performance change. Figure 37 shows an example of the relative module efficiency in dependence of irradiance for the white (C13-D1) and transparent module (C13-E1). The performance curve has been measured with a class A solar simulator equipped with spectral neutral filters for the light attenuation.

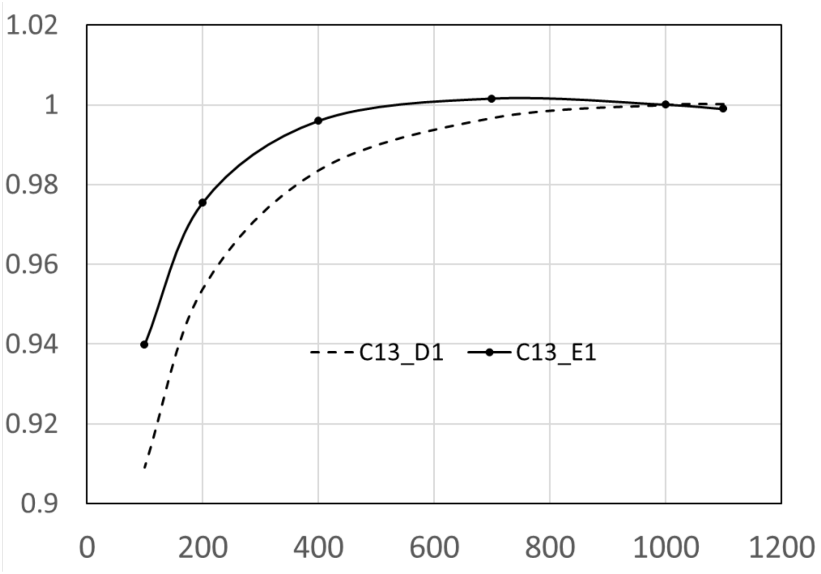

Figure 37: Relative efficiency of the white (D1) and the transparent (E1) module in dependence of irradiance.

For the white module of the 5.5% higher kWh/Wp output respect to its reference module, 3.3% are due to temperature and 2.2% due to spectral and angle of incidence response. The silver module shows as well a positive trend, but much less pronounced due to a lower reflection of the visible spectrum leading to a higher temperature compared to the white module and a lower spectral gain. The red façade module shows to have the highest thermal loss due to higher cell temperatures caused by the very thick glass structure. In the façade module the angular losses have a significant contribution to the calculated L_{Isc}. To separate the spectral from the angle of incidence effect an AOI measurement of the module has to be done. Analysis of this will be continued in a follow up of the project. For the white flag (Appenzell) one would expect a very similar spectral loss as for the silver module. The -7% observed there could be caused by the non-uniformity of the module. Further investigations are here needed.

2.2.3.2. Bifacial modules

Bi-facial PV technology is known to yield from 5% to more than 20% [Singh 2012, Sugibuchi 2013, Chang 2018] additional energy compared to conventional mono-facial modules due to their capability to absorb light through the rear of the module.

The power rating of the bi-facial modules has been recently regulated in January 2019 through the international standard IEC 60904-1-2 where the gain in power generation is determined at different solar irradiances on the rear side of the module. The PV manufacturers of this PV product have adopted quickly the new standard, however the marking and documentation requirements for non-concentrating PV modules, described in the European standard EN50380:2017-09, does not take into consideration the characteristic procedures and supplementary features of bi-facial devices and there is no clear guideline describing the marking procedure.

In a few selected days, this section evaluates the daily energy yielded of bifacial modules in different scenarios including open rack and mounted with white and black diffuse reflectors in the rear of the modules, discuss the main uncertainty contributions when analysing the outdoor performance and assess the main performance indicators.

Non - uniformity

Spectral mismatch and irradiance non-uniformity in the rear of the bi-facial modules are the main source of uncertainties influencing their outdoor measurement accuracy. The evaluation of the spectral impact requires spectrum measurements on the rear of the modules and it is outside the scope of this work, which focuses on the analysis of non-uniform temperature and irradiance distribution over the rear surface of bi-facial modules and its impact on the module performance.

The sensitivity to non-uniformity of irradiance in the rear is complex and depends on the sun's position, the test bench and its surroundings. Figure 38 displays a box plot matrix of the non-uniformity defined as:

$$NU(\%) = 100 \times \frac{G_{max} - G_{min}}{G_{max} + G_{min}}$$

and measured in the rear side of the modules 16-113-A1, 16-074-A2 and 16-074-C3, corresponding to columns A1, A2 and C3 respectively. As mentioned when describing the outdoor test facility, four pyranometers are placed around each bi-facial module so that we can determine the maximum and minimum irradiances, G_{max} and G_{min} respectively, from different measurement points. Each of the three rows in the matrix correspond to day numbers J_d 227, 271 and 331 of the 2018 Julian date calendar. On each box, the central red mark indicates the median, and the bottom and top edges of the box indicate the 25th and 75th percentiles, respectively. The whiskers extend to the most extreme data points not considered outliers, and the outliers are plotted individually using the '+' symbol.

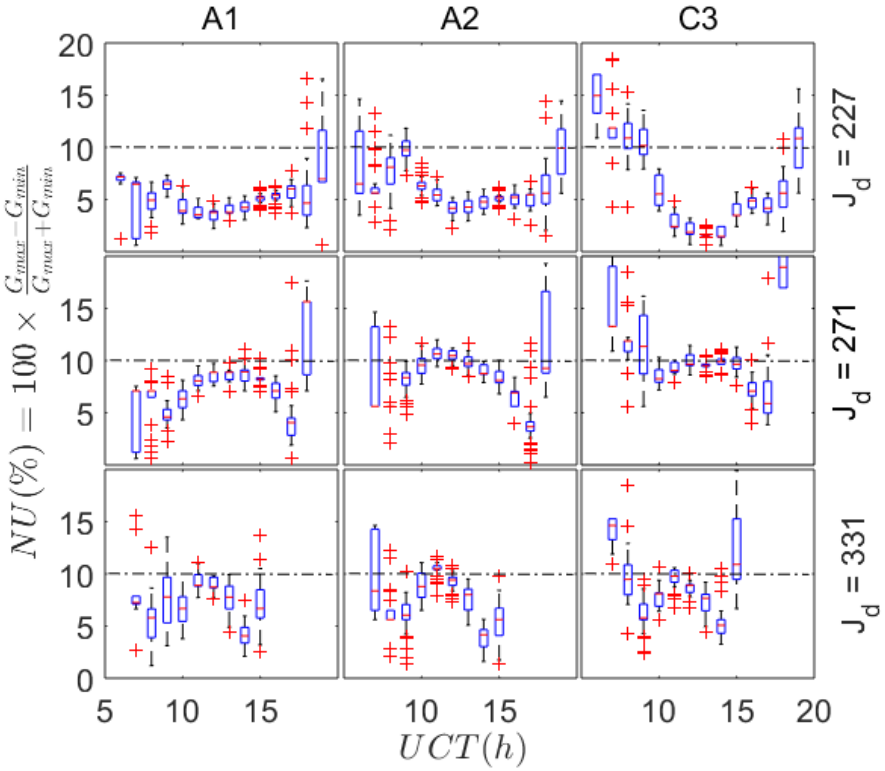

Figure 38: Box plot matrix of non-uniformity of irradiance in the rear of bi-facial modules 16-113-A1, 16-074-A2 and 16-074-C3, corresponding to columns A1, A2 and C3 respectively. Each of the three rows in the matrix correspond to day numbers J_d 227, 271 and 331 of the 2018 Julian date calendar. On each box, the central red mark indicates the median, and the bottom and top edges of the box indicate the 25th and 75th percentiles, respectively. The whiskers extend to the most extreme data points not considered outliers, and the outliers are plotted individually using the '+' symbol.

Please note that the non-uniformity for a specific module depends on the day number of the year, being substantially lower than 10% throughout day 227 (15.08.2018). A defined concave profile is displayed on day number 271 (28.09.2018), where the non – uniformity is close to 10% during the central hours of day. However, the median at lower elevation angles such as in day number 331 (27.11.2018) is closer to 10%. The rows in the plot matrix depict the sensitivity of the radiation uniformity to the position in the test bench, being the first and last hours of the days, with higher angle of incidences, those that have a greater impact on the module's position. In all cases, the uncertainty associated with the non-uniformity of solar irradiance in the rear of the bi-facial modules is greater than the provided by our calibrated broadband detectors.

The power densities that a bi-facial PV module's surfaces record over time are experimentally determined from the irradiance G measurements according to $H_\tau = \int_\tau G\, dt$, where the subscript τ accounts for a specific time intervals such as $\tau = h$ or $\tau = d$ reporting per hour or day respectively. Figure 39 depicts in stacked columns the hourly front solar irradiation H_h^f and mean rear solar irradiation $\overline{H_h^r}$ corresponding to the bi-facial module 16-113-A1 measured on day number 227. In this case, the fraction of mean rear irradiation $\epsilon_{\overline{H_h^r}}$ range from a maximum of 43.9% in the early morning to a minimum of 10.4% at noon in the coordinated universal time, UTC. The dispersion is measured in terms of standard deviation $\sigma_{\overline{H_h^r}}$ and in the above cases correspond to 2.3% and 0.3% respectively.

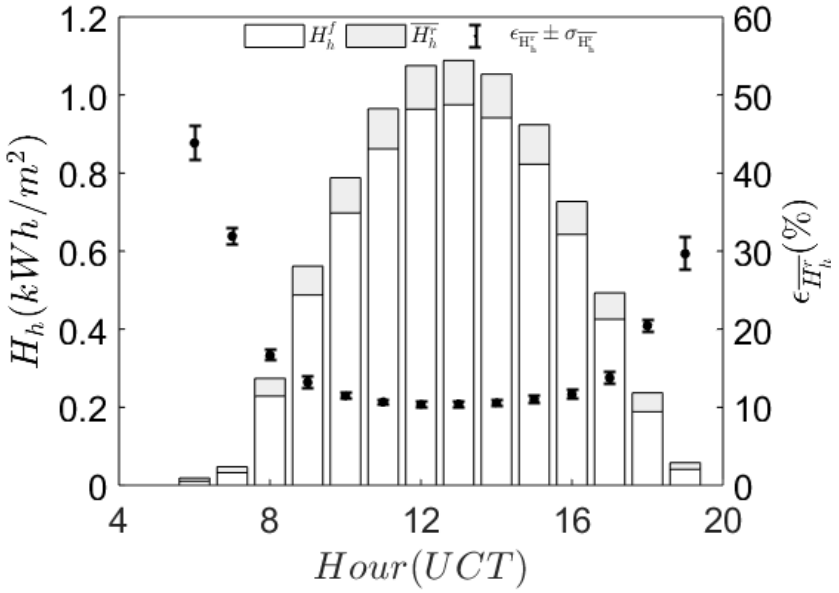

Figure 39: Available solar irradiation at module 16-113-A1 on day number 227. Left *y* axis: columns chart stacking the hourly front solar irradiation H_h^f and mean rear solar irradiation $\overline{H_h^r}$. Right *y* axis: fraction of mean rear irradiation $\epsilon_{\overline{H_h^r}}$ and standard deviation $\sigma_{\overline{H_h^r}}$.

The daily solar irradiation determined at the front and rear surfaces of bi-facial modules 16-113-A1, 16-074-A2 and 16-074-C3 are listed in table 14, where the average fraction of rear radiant energy between modules A1, A2 and C3 is 11.9%, 11.8% and 11.6% respectively in day 227. The non-uniformity of the daily mean irradiation in the rear of the modules is found to be 1.5%. The fraction of rear irradiance in day 331 is reduced to 9.5%, 9.3% and 9.3% respectively, where the non-uniformity remains 0.7%.

Front		Rear A1		Rear A2		Rear C3		
H_d^f	$\cup_{H_d^f}$	$\overline{H_d^r}$	$\cup_{\overline{H_d^r}}$	$\overline{H_d^r}$	$\cup_{\overline{H_d^r}}$	$\overline{H_d^r}$	$\cup_{\overline{H_d^r}}$	
$(kWh \cdot m^{-2})$		$(kWh \cdot m^{-2})$		$(kWh \cdot m^{-2})$		$(kWh \cdot m^{-2})$		# day
7.3189	0.1098	0.9917	0.0359	0.9762	0.0370	0.9616	0.0148	227
6.9489	0.1042	0.7933	0.0565	0.7784	0.0628	0.7724	0.0624	271
4.9532	0.0743	0.5221	0.0298	0.5097	0.0345	0.5086	0.0336	331

Table 13: Front and rear daily solar irradiation of modules 16-113-A1, 16-074-A2 and 16-074-C3 with uncertainties experimentally determined in day numbers 227, 271 and 331.

Module temperature is another key source of uncertainty when determining the main performance indicators in photovoltaics. Analogous to the case of irradiance, the non-uniformity is defined as:

$$NU(\%) = 100 \times \frac{T_{max} - T_{min}}{T_{max} + T_{min}}$$

where the temperature of the modules has been measured in three in different positions in the rear of the modules. Figure 40 depicts the box plot matrix with temperature's non uniformity, where its rows and columns maintain the same logic as in the previous case.

The median of the temperature's non uniformity is found, in general, to be below 5% and values for modules A2 and C3 are systematically below module A1. The inter-quartile ranges (distance between the 75th and 25th percentiles) determine that the non-uniformity spread remains below 1% and just in some specific cases like in the early morning or late afternoon is considerably higher. Our measurement uncertainty in temperature measurements is therefore estimated by considering first the different contributions in the measuring chain with a budget of $\pm 1°C$ and a second contribution accounting for the non-uniformity as discussed above.

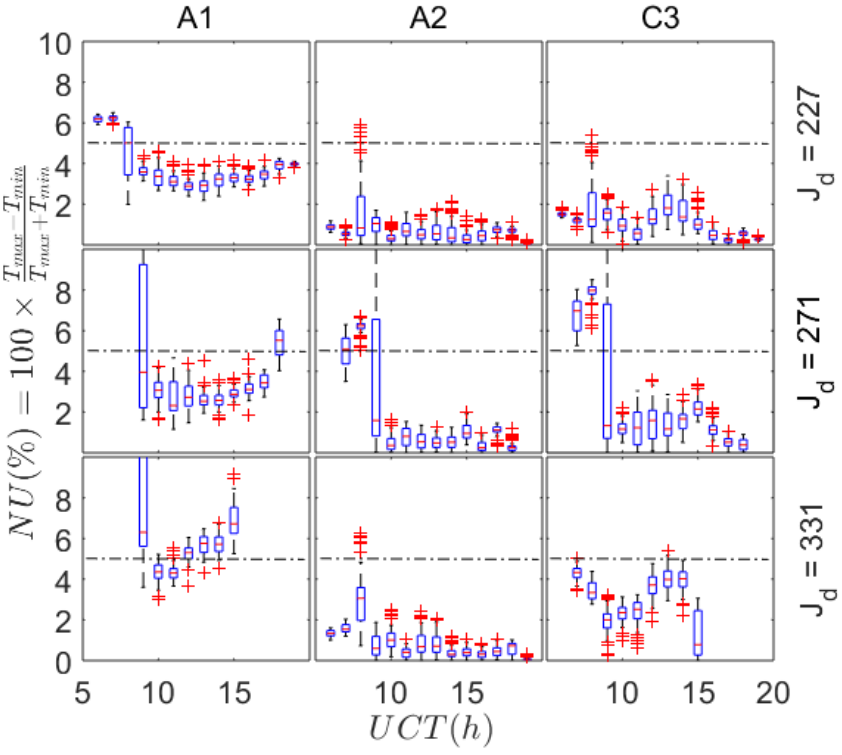

Figure 40: Box plot matrix of non uniformity of temperature distribution in the rear of bi-facial modules. Columns A1, A2 and C3 correspond to modules 16-113-A1, 16-074-A2 and 16-074-C3 respectively. Each of the three rows in the matrix correspond to day numbers J_d 227, 271 and 331 of the 2018 Julian date calendar. On each box, the central red mark indicates the median, and the bottom and top edges of the box indicate the 25th and 75th percentiles, respectively. The whiskers extend to the most extreme data points not considered outliers, and the outliers are plotted individually using the '+' symbol.

Benchmarking of PV modules

The benchmarking of bi-facial PV modules 16-113-A1, 16-074-A2 and 16-074-C3 against the reference crystalline module is based on the energy output calculated as:

$$E = \int P_{max} dt$$

As displayed in figure 41, the assessment of performances requires the normalization of the energy output to a common comparative scale, usually defined as the ratio of energy output to the power rating measured at standard test condition P_{STC} or energy yield Y_a:

$$Y_a = \frac{\int P_{max} dt}{P_{STC}}$$

The specific energy yield Y_a indicates the equivalent amount of time (normally in hours) during which the module would be required to operate at P_{STC} to provide the energy measured during the reporting period.

The three bi-facial modules clearly outperform the crystalline reference module over day number 227 with daily relative differences in energy yield respect to the mono-facial reference of $\epsilon_{Y_a,A1}(\%) = 11.4 \pm 0.2$, $\epsilon_{Y_a,A2}(\%) = 12.2 \pm 0.2$ and $\epsilon_{Y_a,C3}(\%) = 12.5 \pm 0.2$ when using the rated front power measured indoor at standard test condition. The comparison between day numbers 227 and 331 of the selected clear days in table 15 shows a relevant difference from roughly 2% in module 16-113-A1 to 4% in module 16-074-C3, which might be due to seasonal effects.

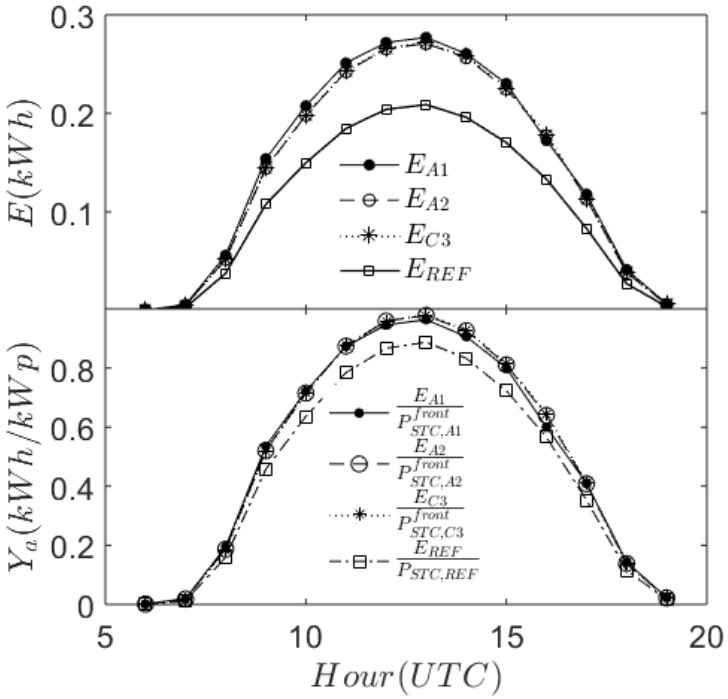

Figure 41: Hourly energy output E (top) and energy yield Y_a (bottom) of bi-facials and reference crystalline PV module over the day number 227.

Day number	$\epsilon_{Y_a,A1}(\%)$	$\epsilon_{Y_a,A2}(\%)$	$\epsilon_{Y_a,C3}(\%)$
227	11.4 ± 0.2	12.2 ± 0.2	12.5 ± 0.2
271	10.3 ± 0.2	11.5 ± 0.2	11.7 ± 0.2
331	9.6 ± 0.2	9.0 ± 0.2	8.7 ± 0.2

Table 14: Daily relative differences in energy yield of modules 16-113-A1 ($\epsilon_{Y_a,A1}$), 16-074-A2 ($\epsilon_{Y_a,A2}$) and 16-074-C3 ($\epsilon_{Y_a,C3}$) respect to the mono-facial reference

PV modules, including bi-facials, are typically sold in price per watt peak W_p and therefore the marking including nameplate and documentation stating the power rating of the module acquire great relevance when assessing the most suitable PV module for a specific application. The marking and documentation requirements for non-concentrating PV modules are described in the European standard EN50380:2017-09 and it does not take into consideration the characteristic procedures and supplementary features of bi-facial devices that was published in the IEC 60904-1-2 January, 2019. In this standard procedure, the gain in power generation yielded by the bi-faciality of the device is determined at different solar irradiances on the rear side of the module according to the equivalent irradiance defined as:

$$G_{Ei} = G_{STC}1000\ W \cdot m^{-2} + \varphi \cdot G_{Ri}$$

where G_{STC} is the $\varphi = Min(\varphi_{I_{sc}}, \varphi_{P_{max}})$ is the bi-facial coefficient and G_{Ri} the rear side irradiance level i. From this characteristic features, the bifaciality, two specific maximum powers corresponding to P_{GE10} and P_{GE20}, accounting for $G_{R1} = 100\ W \cdot m^{-2}$ and $G_{R2} = 200\ W \cdot m^{-2}$ respectively, must be reported.

Field performance of bi-facial modules greatly depends on the rear side irradiance and module type and therefore consumers require additional power labelling information to differentiate the products. As stated in table 9, the main electrical characteristics of the crystalline reference module 14-I03-C4 and bi-facials 16-113-A1, 16-074-A2 and 16-074-C3 are quite similar and consistent with the same cell technology, especially between the reference and the 16-113-A1. We have already seen in figure 41 that this bi-facial module installed in Lugano in the configuration described in section 2.3.1 yields (depending on the day number) between 9.6% to 11.4% more than the reference one when both are rated equally as mono-facials at STC.

The enhanced energy yield from bi-facial modules might justify and bring a slight increase in price of this technology, but the assessment of how much is it worth paying for strongly depend on the mounting conditions and surroundings as described in [Deline 2017]. Figure 42 compares the energy yield of the crystalline reference with the bi-facial 16-113-A1 as if it had been commercially priced as an equivalent peak power corresponding to standard test conditions P_{STC} or matching P_{GE10} and P_{GE20}. The boosted energy in the first case has already been discussed above, but please note that the energy yield obtained as if the module had been commercially priced as an equivalent peak power of P_{GE10} still accounts for a light outperforming of $\epsilon_{day}(\%) = +2.17 \pm 0.03$ in day number 227. Therefore, from the results listed in table 16, we can conclude that bi-facial module 16-113-A1 outperform the crystalline reference 14-I03-C4 (with similar cell performance) from 2.17% in day number 227 to 0.54% in day number 331 when the bi-facial module is rated as P_{GE10} instead of P_{STC}, installed in Lugano and under clear days. The module underperform below -5% when rated as P_{GE20} and monitored under the same mounting and weather conditions.

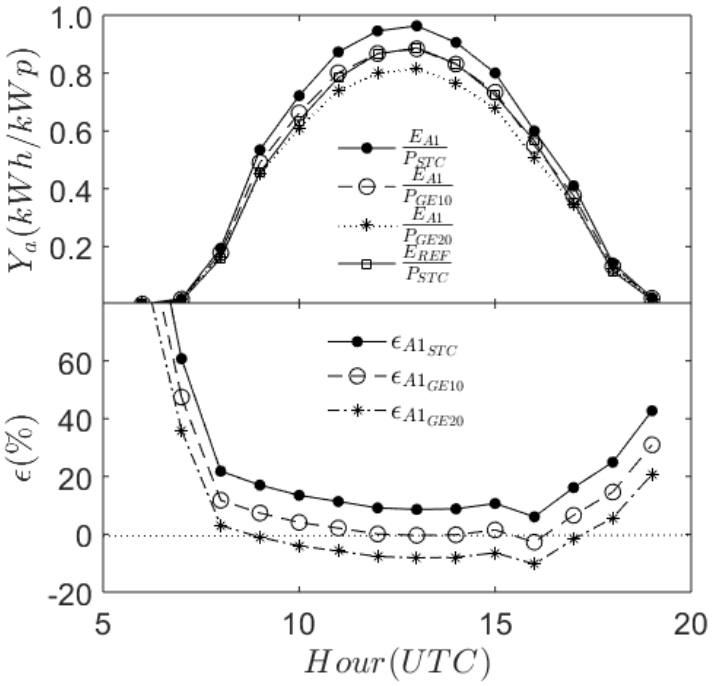

Figure 42: Hourly energy yield Y_a (top) and relative difference between the reference crystalline and the energy yield of the 16-113-A1 bi-facial module (bottom) over day number 227.

Day number	$\epsilon_{Y_a,A1}^{STC}(\%)$	$\epsilon_{Y_a,A1}^{GE10}(\%)$	$\epsilon_{Y_a,A1}^{GE20}(\%)$
227	$+11.4 \pm 0.4$	$+2.17 \pm 0.07$	-5.8 ± 0.2
271	$+10.3 \pm 0.4$	$+1.16 \pm 0.04$	-6.7 ± 0.2
331	$+9.6 \pm 0.3$	$+0.54 \pm 0.02$	-7.3 ± 0.2

Table 15: Daily relative differences in energy yield respect to the mono-facial reference 14-I03-C4 when the bi-facial module 16-113-A1 is rated as P_{STC} P_{GE10} and P_{GE20}.

As the geographic location and local mounting have a relevant influence in the solar irradiation H, comparison between modules receiving different irradiances are normally addressed through the module performance ratio MPR. Defined first at system level in [IEC 61724-1] and later at module level in [IEC 61853-3], it relates the utilizable energy to the amount of energy which could be generated in case modules were operated under STC. It represents the ratio of specific energy yield Y_a to so-called reference yield Y_r.

$$MPR = \frac{Y_a}{Y_r} = \frac{E}{P_{STC}} \times \frac{1000W/m^2}{H}$$

The specific energy yield Y_a has already been defined as the ratio of the output energy to the module power rating at standard test condition P_{STC}. It indicates the equivalent amount of time (normally in hours) during which the module would be required to operate at P_{STC} to provide the energy measured during

the reporting period. The reference yield stands for the number of hours during which the solar radiation would need to be at reference irradiance levels in order to contribute the same incident solar energy. If the reporting period were one day, then Y_r would be the equivalent number of sun hours at the reference irradiance per day.

Figure 43 compares, in day number 227, the performance ratio of the crystalline reference with the bi-facial module 16-113-A1 as if had been commercially priced as an equivalent peak power corresponding to P_{STC}, P_{GE10} or P_{GE20}. The MPR calculated for the bi-facial module at standard test condition is higher than the crystalline reference module. By integrating over the whole day and taking uncertainties into account results are $MRP_{REF,STC} = 0.89 \pm 0.04$ and $MRP_{A1,STC} = 0.99 \pm 0.04$ respectively. If the bi-facial would had been commercially rated as P_{GE10} or P_{GE20}, the performance ratios are $MRP_{A1,GE10} = 0.91 \pm 0.04$ and $MRP_{A1,GE20} = 0.84 \pm 0.04$ respectively. This result is consistent to the obtained for the energy yield where values corresponding to the reference crystalline and the bi-facial rated as P_{GE10} were similar and values for the P_{GE20} underperforms. Daily relative differences listed in table 17.

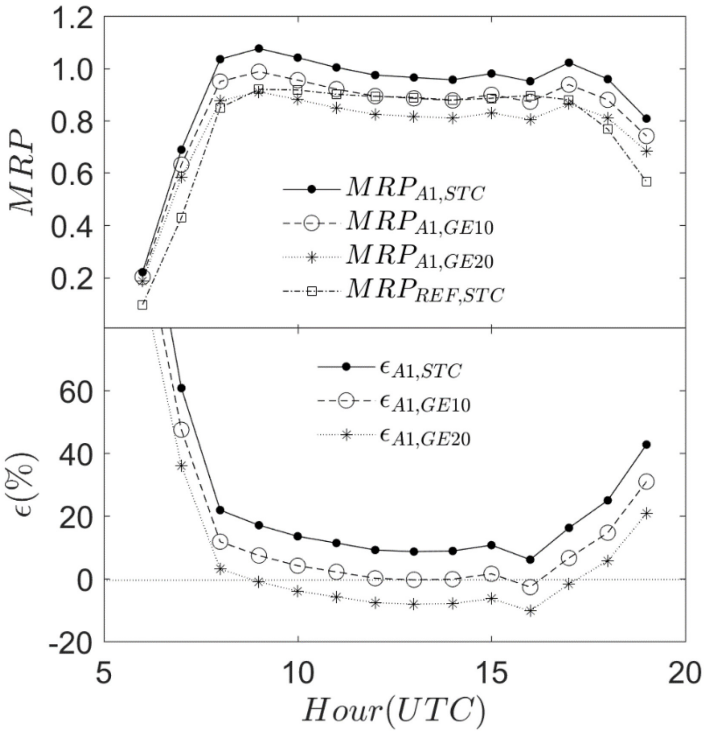

Figure 43: Hourly module performance ratio MPR (top) and relative difference between the reference crystalline and the MPR of module 16-113-A1 (bottom) over day number 227.

Day number	$\epsilon^{STC}_{MPR,A1}(\%)$	$\epsilon^{GE10}_{MPR,A1}(\%)$	$\epsilon^{GE20}_{MPR,A1}(\%)$
227	$+11.1 \pm 1.0$	$+2.2 \pm 0.2$	-5.8 ± 0.5
271	$+10.3 \pm 0.9$	$+1.2 \pm 0.1$	-6.7 ± 0.6
331	$+9.6 \pm 0.9$	$+0.54 \pm 0.05$	-7.3 ± 0.7

Table 16: Daily relative differences in module performance ratio respect to the mono-facial reference 14-I03-C4 when the bi-facial module 16-113-A1 is rated as P_{STC}, P_{GE10} and P_{GE20}.

The strong dependence of MPR on temperature results in large seasonal variation of about two percent points. The temperature-corrected PR results in a more consistent result through the year and therefore MPR is often corrected to a common temperature of 25°C, [Ishii 2011a, Ishii 2011b] according to

$$MPR_{25} = \frac{MPR}{[1 + \delta(\langle T \rangle - 25)]}$$

where $\langle T \rangle$ is the weighted average temperature defined as

$$\langle T \rangle = \frac{\int_\tau TGdt}{\int_\tau Gdt}$$

and τ is the integration interval in which the average is made. Please note that uncertainties related to non-uniformities have been also weighted analogously with the irradiance and results are listed in table 18.

Day number	$\epsilon^{STC}_{MPR25,A1}(\%)$	$\epsilon^{GE10}_{MPR25,A1}(\%)$	$\epsilon^{GE20}_{MPR25,A1}(\%)$
227	$+9 \pm 1$	$+0.42 \pm 0.01$	-7 ± 1
271	$+10 \pm 2$	$+1.1 \pm 0.1$	-6.8 ± 0.2
331	$+10 \pm 2$	$+0.50 \pm 0.08$	-7 ± 1

Table 17: Daily relative differences in module performance ratio corrected to a 25°C and respect to the mono-facial reference 14-I03-C4 when the bi-facial module 16-113-A1 is rated as P_{STC}, P_{GE10} and P_{GE20}.

Bi-facial PV modules with rear panels

As the bi-facial modules absorb sunlight from the rear, the effect of a white rear panel as diffuse reflector has been investigated as an alternative strategy to the classic white ground material. As depicted in figure 44, this configuration might be associated with applications into the built environment, where the white rear surfaces might act as rooftops or wall reflectors.

Figure 44: White diffuse reflectors mounted in the rear of bi-facial PV modules: front (left) and side (right) view.

The hourly front solar irradiation H_h^f and mean rear solar irradiation $\overline{H_h^r}$ of bi-facial module 16-113-A1 with white reflectors mounted at distance $d = 38.5\ cm$ on day number 423, is compared in figure 45 with the solar irradiation recorded when the reflectors were replaced with black panels as reference at the same distance on day number 447. The fraction of mean rear radiant energy with white reflectors is considerably higher than with the black reflectors, representing 29.6% and 5.1% respectively. As in the case with no reflectors in the rear of the modules, the mean daily non-uniformity is calculated by integrating the measured rear irradiance for the whole day, being 26.0% and 8.7% for white and black panels respectively. Table 19 lists the front and rear daily solar irradiation of bi-facial modules 16-113-A1, 16-074-A2 and 16-074-C3 with the corresponding uncertainties at module to reflector distances of 75.5 cm, 48.5 cm and 38.5 cm.

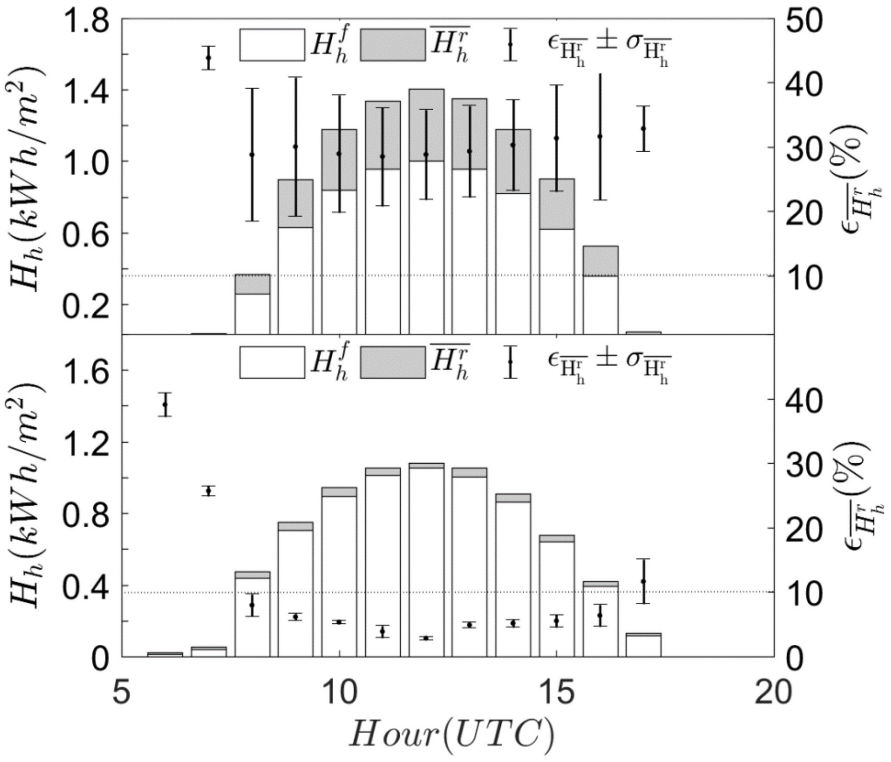

Figure 45: Available solar irradiation at module 16-113-A1 when white (top) and black (bottom) reflector panels are mounted in the rear of bi-facial modules on day numbers 423 and 447 respectively. Left y axis: columns chart stacking the hourly front solar irradiation H_h^f and mean rear solar irradiation $\overline{H_h^r}$. Right y axis: fraction of mean rear irradiation $\epsilon_{\overline{H_h^r}}$ and standard deviation $\sigma_{\overline{H_h^r}}$.

Front		Rear A1		Rear A2		Rear C3				
H_d^f	$\cup_{H_d^f}$	$\overline{H_d^r}$	$\cup_{\overline{H_d^r}}$	$\overline{H_d^r}$	$\cup_{\overline{H_d^r}}$	$\overline{H_d^r}$	$\cup_{\overline{H_d^r}}$		d	
$(kWh \cdot m^{-2})$		$(kWh \cdot m^{-2})$		$(kWh \cdot m^{-2})$		$(kWh \cdot m^{-2})$		# day	(cm)	Reflector
4.73	0.07	1.6	0.8	1.6	0.8	1.6	0.8	342	75.5	White
4.29	0.06	1.7	0.9	1.7	0.8	1.8	0.9	372	48.5	
6.5	0.1	2.7	0.7	2.7	0.7	2.8	0.8	423	38.5	
7.2	0.1	0.41	0.03	0.39	0.03	0.40	0.02	447	38.5	Black
7.5	0.1	0.6	0.2	0.5	0.2	0.6	0.1	506	75.5	
6.9	0.1	0.4	0.2	0.4	0.2	0.4	0.2	508	48.5	

Table 18: Front and rear daily solar irradiation of modules 16-113-A1, 16-074-A2 and 16-074-C3 with uncertainties experimentally determined.

As displayed in figure 46, both type of reflectors (white and black) increases the non-uniformities in irradiance with respect to the initial configuration without any reflector on the rear of the modules, and reaching instant values considerable higher than 10% and therefore, worsen the overall uncertainty. The main difference between matrices of non-uniformities with white and black reflectors lies in the early morning and late afternoon, where reflections coming from the white panels are higher at any of the tested distances regardless the position of the bi-facial module.

The non-uniformities in temperature are shown in figure 47, remaining generally below 5% except for module A1 in day number 342 (with white reflector) that displays instant values between 5% and 10%. No significant differences over the temperature distribution with respect to the type of mounted reflector has been found.

The effect of the reflector's distance to the PV modules is clearly observed at $d = 38.5\,cm$, where the irradiance's non-uniformity is reduced, for both white and black reflectors, respect to longer distances such as $d = 48.5\,cm$ or $d = 75.5\,cm$.

Comparing the performance ratios MPR of the bi-facial modules with white reflectors against the crystalline reference and normalizing at 25°C, it is observed that the daily relative differences at standard test conditions are in general above +20%. It reaches only up to 15% just in the case of module 16-113-A1 when the distance between the reflector and the module is 38.5 cm on day number 423. Since the available irradiation in the rear is higher than in day numbers 342 and 372, the relative difference respect to the reference would be greater and therefore this result is unexpected. If the bi-facial module 16-113-A1 had been commercially rated as P_{GE10} and P_{GE20} instead of standard test conditions, it still outperforms the reference crystalline with relative differences above +10% and +3% for $GE10$ and $GE20$ respectively. In the case of reflector distance of 38.5 cm, the relative difference in MPR is considerable reduced. Further investigations including simulations and long-term analysis of performance evolution over time should be carried out in order to detailed analysis the impact of the non-uniformity over the electro-thermal performance of the modules.

The comparison with black rear reflectors shows that bi-facial modules still outperform the mono-facial reference when rated at standard test conditions. However, bi-facial modules would underperform if they were commercially rated either as P_{GE10} or P_{GE20}. The daily relative differences in module performance ratio are listed in table 20.

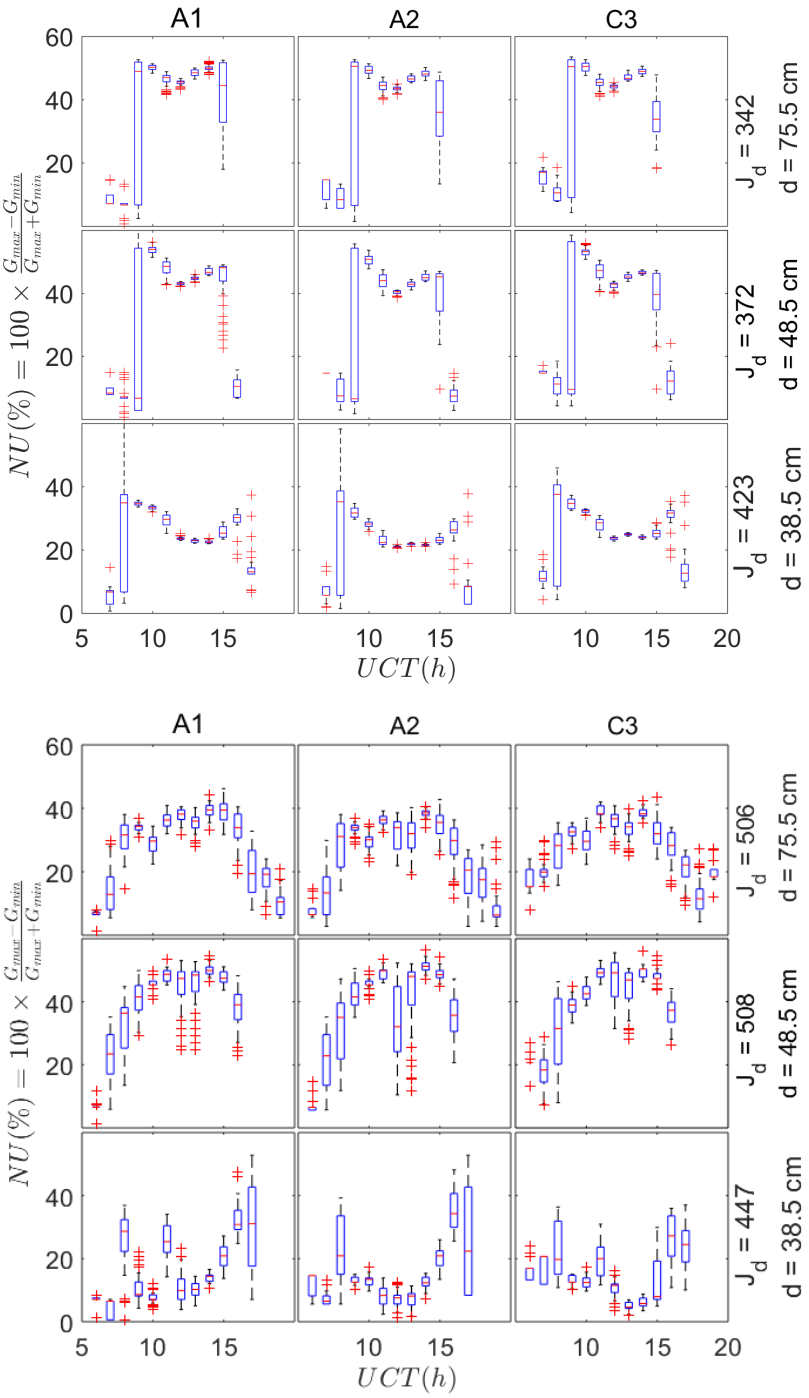

Figure 46: Box plot matrices of irradiance non-uniformities of bi-facial modules 16-113-A1, 16-074-A2 and 16-074-C3, corresponding to columns A1, A2 and C3 respectively. (Top) White and (bottom) black panels installed behind the modules at distances of $d = 75.5\ cm$, $d = 48.5\ cm$ and $d = 38.5\ cm$. Each of the three rows in each matrix correspond to a specific day number of the Julian date calendar $J_d$and the respective panel distances. On each box, the central red mark indicates the median, and the bottom and top edges of the box indicate the 25th and 75th percentiles, respectively. The whiskers extend to the most extreme data points not considered outliers, and the outliers are plotted individually using the '+' symbol.

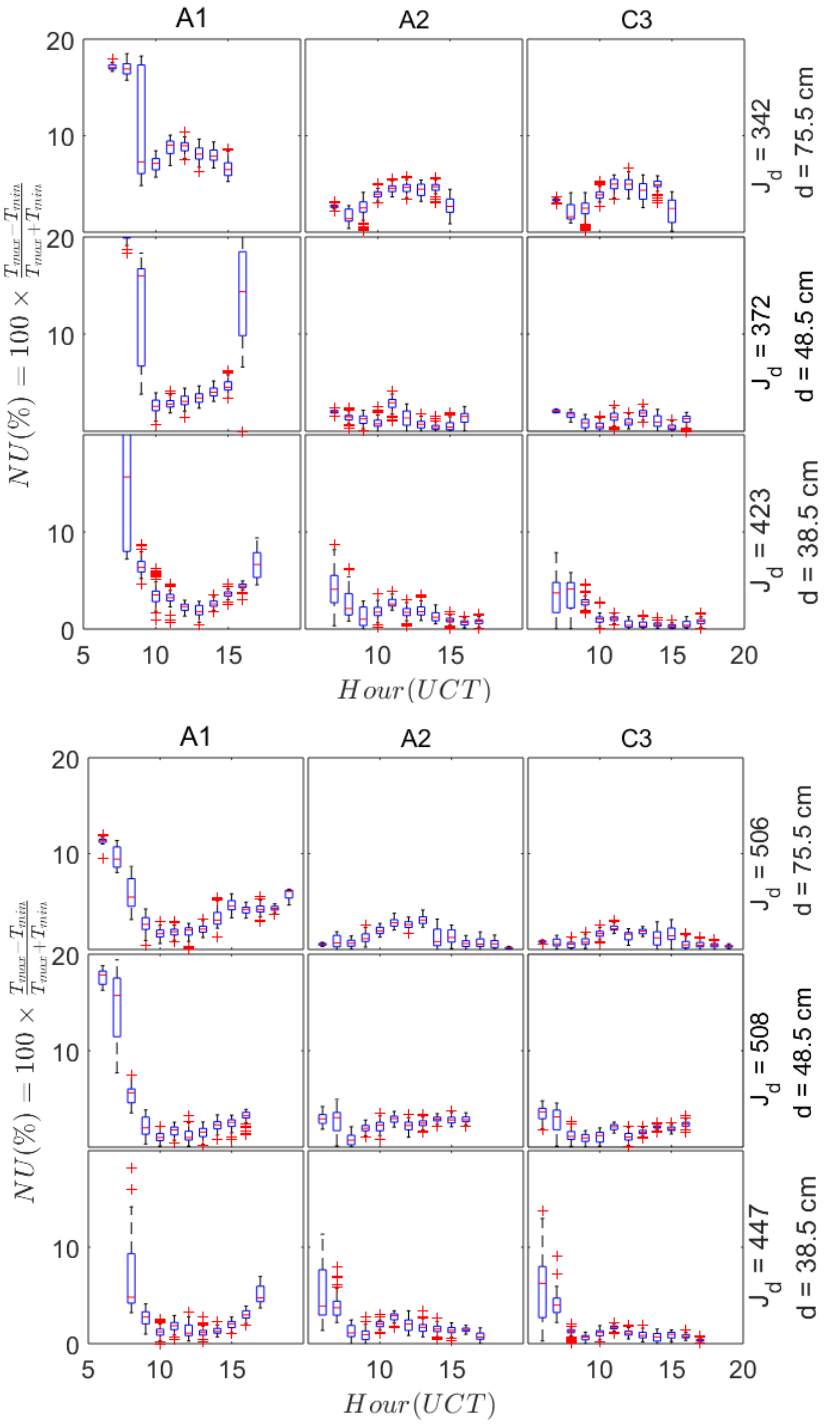

Figure 47: Box plot matrix of temperature's non uniformity distributed in the rear of bi-facial modules 16-113-A1, 16-074-A2 and 16-074-C3, corresponding to columns A1, A2 and C3 respectively. (Top) White and (bottom) black panels installed behind the modules at distances of d=75.5 cm, d=48.5 cm and d=38.5 cm. Each of the three rows in the matrix correspond to day numbers of the Julian date calendar J_d and the respective panel distances. On each box, the central red mark indicates the median, and the bottom and top edges of the box indicate the 25th and 75th percentiles, respectively. The whiskers extend to the most extreme data points not considered outliers, and the outliers are plotted individually using the '+' symbol.

	d (cm)	Day number	$\epsilon^{STC}_{MPR25,A1}(\%)$	$\epsilon^{GE10}_{MPR25,A1}(\%)$	$\epsilon^{GE20}_{MPR25,A1}(\%)$	$\epsilon^{STC}_{MPR25,A2}(\%)$	$\epsilon^{STC}_{MPR25,C3}(\%)$
	75.5	342	$+22 \pm 9$	$+12 \pm 5$	$+3 \pm 1$	$+22 \pm 8$	$+23 \pm 8$
	48.5	372	$+22 \pm 9$	$+12 \pm 5$	$+3 \pm 1$	$+22 \pm 8$	$+23 \pm 9$
	38.5	423	$+15 \pm 5$	$+5 \pm 2$	$+3 \pm 1$	$+19 \pm 6$	$+21 \pm 7$
	38.5	447	$+1.3 \pm 0.2$	-7 ± 1	-14 ± 2	$+4.1 \pm 0.5$	$+4.1 \pm 0.5$
	75.5	506	$+4.5 \pm 0.7$	-4.2 ± 0.6	-12 ± 2	$+6.7 \pm 0.9$	$+8 \pm 1$
	48.5	508	$+3.4 \pm 0.5$	-5.2 ± 0.7	-13 ± 2	$+6.2 \pm 0.9$	$+6.2 \pm 0.9$

Table 19: Daily relative differences in module performance ratio respect to the mono-facial reference 14-I03-C4 and corrected to a 25°C when the bi-facial module 16-113-A1 is rated as P_{STC}, P_{GE10} and P_{GE20} and modules 16-074-A2 and 16-074-C3 rated as P_{STC}.

2.3 Procedures and equipment

Background:

The results from the test challenges of the new generation photovoltaics and requirements for the outdoor performance and modelling will give feedback to upgrade the existing indoor and outdoor testing equipment and test procedures which flows into normative activities in which SUPSI is involved at IEC level.

Scope of the project:

- Test new equipment for electrical and optical measurements.
- To upgrade the indoor equipment and test procedures allowing to maintain a leading role at national and international level
- Upgrade the outdoor equipment to meet the measurement challenges coming from the test challenges of the new generation and novel technologies
- To cooperate in the development of new or review of existing international testing standards

Results:

- A new test-bench based on a 1-axis stage that rotates from -90° to +90° was designed and set-up to analyze and assess the angle of incidence dependences of solar cells.
- The test procedure and measurement uncertainty for the angular loss analysis at cell level was validated through the participation in an international round-robin.
- SUPSI exchanged experience and know-how on indoor and outdoor measurement procedures within the technology collaboration programme, IEA Task 13, for the performance, operation and reliability of photovoltaic systems. SUPSI also joined the sub-team AoI at the working group 2 of the technical committee 82 in order to cooperate in the review of the international standards IEC 61853-2.

2.3.1 New set-up for angular loss analysis

2.3.1.1. Introduction

The fraction of irradiance available for conversion into electric current depends on the angle between the direct solar radiation and the normal direction of the PV panel and the purpose of the incident angle test is to determine the influence of the solar angles of incidence on the module performance. Recognizing that the PV modules are typically rated just at standard test conditions, STC, the IEC Technical Committee 82 Working Group 2 (TC 82/WG 2) has developed a power and energy rating standard, IEC 61853-2, describing the procedures for measuring the performance effect of angle of incidence. A new set-up and procedure developed at SUPSI-ISAAC for angular loss analysis is being developed within this work.

2.3.1.2. Equipment

The indoor characterization procedure using simulated sunlight developed at SUPSI-ISAAC is compatible with two different types of lighting systems. The first option is based on a Xe flash lamp generating a light pulse with a plateau of about 10 ms on which the spectral irradiance approximates the reference solar spectra irradiance AM1.5G with a spectral match, spatial non-uniformity and temporal instability rated as A+A+A+ according to the IEC 60904-9 standard. The second lighting system is conceived for the estimation of the relative angular-dependent spectral responsitivity RADSR and uses another Xe flash lamp with a set of band-pass filters ranging from 311 nm to 1098 nm.
The active surface of the devices under test DUT are mounted coplanar with a calibrated cell on a custom designed rack, which accommodates PV devices in sizes up to 1.5 x 2.0 m2. The structure is equipped with a single automated rotation shaft which is DUT centered and perpendicular to the optical axis. It provides tilt θ adjustment from -90° to +90°.
The electronic load of the solar simulator measures the IV-curve of the DUT, the intensity of the simulated sunlight and temperatures of DUT and reference cell. The angle of incidence AoI measurements are performed in a dark room equipped with an active temperature control system in order to guarantee that the relative light transmission $\tau(\theta)$ is calculated according to the standard test conditions STC.
The new rack structure displayed in figure 48 has been designed in order to ensure that the structure holds at least 50 kg of modules, which double the weight of normal double glass modules, and the tip displacement of the profiles remains below 1mm in the worst-case scenario. The rotation is driven by a nema 34 step motor with a bipolar holding torque of 8.9 Nm that transmit the motion and force through a timing belt system. The transmission system has one pulley rigidly mounted on the drive shaft of the step motor and another pulley mounted on the driven shaft of the photovoltaic mounting structure connected by a timing belt. The pulleys have different number of teeth as to reduce the input speed of the driver shaft and rise the torque or turning force of the driven pulley by a factor 3. The electronic driver of the step motor is set with a resolution of 0.18° under the micro-step configuration of 2000 steps per revolution. A 12-bit absolute (4096) position rotary encoder have been also mounted on the driven shaft, which is DUT centered, in order to determine the position of the PV module by using a static reference point. It delivers a high quality feedback for accurate motion detection. The rotation has been automated and controlled by computer through a tailor-designed software.

Figure 48: Rack mounting structure for the angular loss analysis of PV modules in sizes up to 1.5 x 2.0 m2

2.3.1.3. Uncertainty calculation

The test method for the incident angle test is based on gathering actual measured I_{sc} data for the test modules over a wide range of incidence angles. The measurement process itself consists in the determination of irradiance, temperature and short-circuit current of the PV module according to:

1. At 0° rotation angle position the test cell in the test area so that the center of the cell lies in the optical axis and the axis of rotation in the middle of the cell. Rotational symmetry of the test arrangement shall be verified at –80° and 80° rotation angle. The ratios $I_{sc}(80^{\circ})/[I_{sc}(0^{\circ}) \times cos(80^{\circ})]$ for both directions shall not differ by more than 2 %.
2. Vary the angle between the module normal and the optical axis of the light source between -85° and + 85° in steps of a maximum of 5°.
3. The relative light transmission into the module is given by:

$$\tau(\theta) = I_{sc}(\theta)/[I_{sc}(0°) \times cos(\theta)]$$

where θ corresponds to the angle of incidence with respect to the module normal.
The most important contributions to uncertainty with regard to the measurement and evaluation process are summarized in figure 49.

Electrical measurements

The sources of uncertainty in the electrical measurements are the data acquisition channels for the measurements of irradiance and current. The manufacturer states a Gaussian contribution to uncertainty in all measurement ranges, being ± 0.023 % the worst-case scenario.

Temperature

Temperature sensors or probes returns a temperature-dependent signal, which is transmitted, to the evaluation electronics where it is finally converted into a temperature indicator or a current signal. The uncertainty of the probes is estimated in ± 0.18 °C and follows a Gaussian distribution with a 95% confidence interval. The data acquisition system states a Gaussian uncertainty with a 99% confidence interval on a temperature indicator of ± 0.5 °C.

The devices under test are thermalized at 25.0 ±0.5°C in the laboratory prior the measurements and the uncertainty in temperature is assumed to be uniformly distributed within ± 0.5 °C.

Geometric optics

The main contributions to uncertainty in geometric optics are the relative orientation of the test device or angle of incidence, alignment between the test device and reference cell, spatial non-uniformity and spectral mismatch for best uncertainty. The maximum deviation of the angle of incidence α from normal incidence is determined according to

$$\alpha = arctan\left(\frac{R}{L}\right) = 5.36°$$

where $L = 8.0\ m$ is the distance solar simulator - target plane and $R = 0.75\ m$ is the maximum distance of the reference cell from the center of the target plane. From the geometry defining the maximum angle of incidence, the uncertainty distribution is assumed to be triangular. The maximum misalignment between the module and the reference cell is assumed to be 3°, with uniform uncertainty distribution and the spatial non-uniformity of the illumination on the declared test plane area is periodically checked according to IEC 60904-9 to be below ± 1%. This error distribution is considered to be uniformly distributed. Finally, the uncertainty over the spectral mismatch is affected by the spectral irradiance of the solar simulator and the spectral responses of the device under test and reference cell. Its estimation is based on Hohl-Ebinger and Warta approach [Hohl-Ebinger 2011] and evaluated as ± 0.5 % within a 99 % confidence interval.

Reference cell

Primary reference cells are calibrated periodically by an external calibration laboratory with a stated uncertainty of ± 0.5 % with Gaussian distribution and 95% confidence interval (or coverage probability). The calibrated value of the reference cell is not adjusted at each calibration, but only when deviations are higher than 0.224%, measured from the moving average calculated upon historical values of 3 primary reference cells calibrated annually since 7 to 11 years. The deviation includes possible drifts of the calibration values and the error arising from the choice of not adjusting the calibration value at each calibration. The uncertainty associated with the measurements of shunt resistors follows a rectangular distribution. Devices with deviations from the calibration value greater than ± 0.1 % are dismissed.

Repeatability

Periodical measurements are performed to prove overall stability in the measurement system. The maximum deviation found from the mean short-circuit current measured on various reference modules is ± 0.243%.

The above described contributions determine an uncertainty budget that is summarized in table 21

$\boldsymbol{\theta}(°)$	**0**	**10**	**20**	**30**	**40**	**50**	**60**	**65**	**70**	**75**	**80**	**85**
$\boldsymbol{u[\tau(\theta)]}$	5.0	5.2	5.5	5.8	6.2	6.7	7.4	8.0	8.8	10.2	12.9	20.9

Table 20: Uncertainty budget estimated for rotation angles from 0° to 85° in steps of a maximum of 10°.

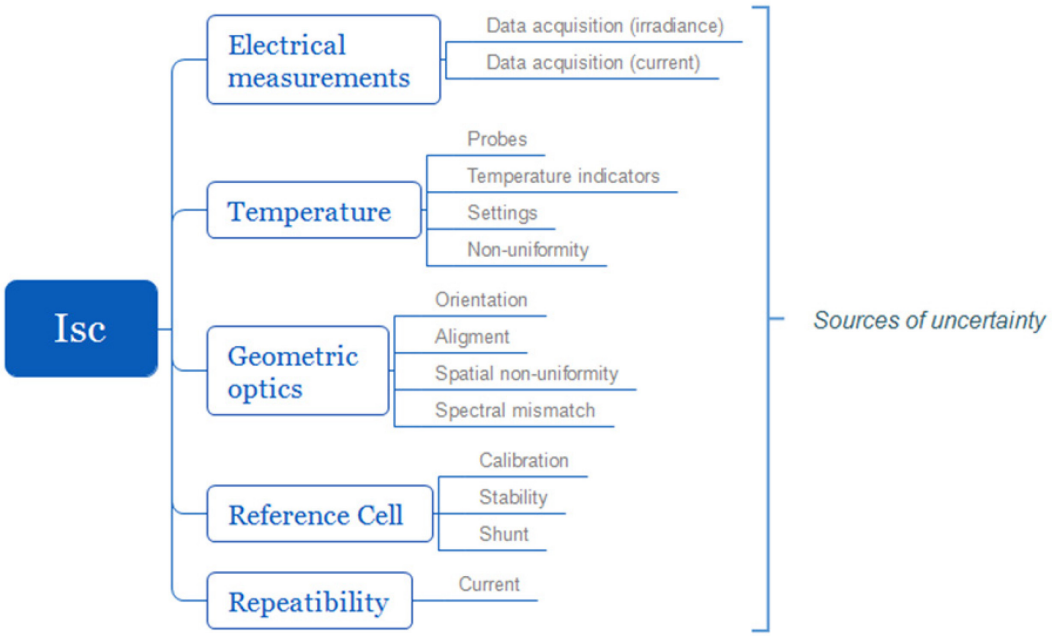

Figure 49: Sources of uncertainty in the new set-up for angle of incidence, AoI, measurements at SUPSI-ISAAC

2.3.1.4. Validation of the measurement procedure – Round Robin at cell level

The core objective of the round-robin is to determine the level of agreement in the measurement results performed at each laboratory at each angle of incidence. The range of angles to be measured extends from – 85° to + 85°. The results will be analyzed using the En number statistical approach as outlined in ISO 17043:2010.

There are eight scientific institutions from six European countries involved in the measurement comparison. These partners include the Department of Photonics Engineering at the Technical University of Denmark (DTU), Physikalisch-Technische Bundesanstalt (PTB), the Energy Research Centre of the Netherlands (ECN), the Centre for Renewable Energy Systems Technology (CREST) at Loughborough University, the Spanish National Renewable Energy Centre (CENER), the Renewable Energy Division at CIEMAT and the University of Applied Sciences and Arts of Southern Switzerland (SUPSI-ISAAC)

The measurement systems used at CREST, ECN, Fraunhofer ISE and SUPSI are based on an indoor flash system used for full-sized modules, but the rotation stage uses different approach. ECN is only capable of holding small laminates in size up to 20 x 20 cm while CREST, FhG ISE and SUPSI can accommodate up to full-sized modules. CENER has a two-axis tracker for characterization that can accommodate up to full-sized module for outdoor measurements. The Ciemat, DTU and PTB systems are only capable of accommodating single cell laminates up to 156 x 156 mm.

Three different PV devices under test, DUT, in duplicate are included in the round-robin, i.e. each lab measures six DUTs in the total. Redundant samples were used so there would always be a backup in the case that any one sample became damaged. All DUTs have the following specifications: (i) An active cell area of 156 mm x 156 mm; (ii) full area dimensions of 200 mm x 200 mm; (iii) 3.2 mm thick finely textured PV glass superstrate, (iv) two tabs as metal contacts; and (v) a flat back sheet surface, which becomes rounder toward the edges. The differences between the DUTs are the cell types and cell texturing. Two DUTs are mono-crystalline standard silicon; two DUTs are multi-crystalline black silicon textured under reactive ion etch (RIE) treatment (referred to as ‘Black-Si A’ hereafter); and two DUTs

are multi-crystalline black silicon textured under atmospheric pressure dry etching (ADE) treatment textured (referred to as 'Black-Si B' hereafter). The edges of samples were taped off to prevent measurement artefacts at large incident angles.

Initial results discussed in [Riedel 2018] highlighted discrepancies between SUPSI's angular transmission measurement τ and the reference value obtained as the weighted mean of all partner's measured τ values. Differences in measurements were believed to be due to misalignment and unwanted reflections and therefore the alignment has been adjusted, the diaphragms have been regulated in order to minimize reflections within the dark room and obstacles behind the mounting rack have been removed. The impact of each action over the angular transmission of the devices is displayed in figure 50.

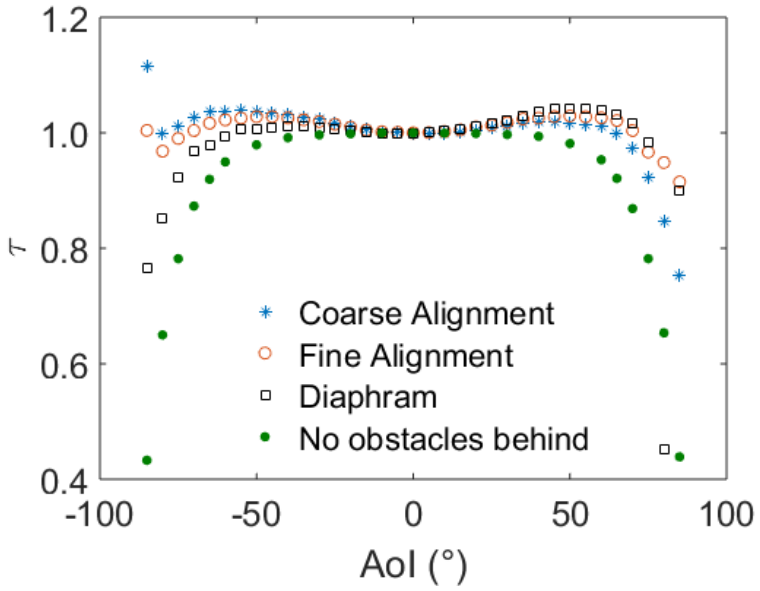

Figure 50: Overlay of transmission as a function of the angle of incidence AoI measured after actions of alignments, regulation of diaphragms and removal of obstacles behind the rack.

The expanded uncertainty provided from each partner laboratory is shown as a function of the angle of incidence, AoI in Figure 51. A trend of increasing uncertainty with increasing AoI, wherein a range of 0.1% to 5% at normal incidence and a range of 2.5% to 20.9% at 85° AoI is observed. The specific reasons for this increasing trend will be unique to a given measurement system (e.g. increasing non-uniformity or uncertainty of the measured angle θ). The uncertainty budget at SUPSI has been overestimated as a conservative approach, especially at low angle of incidence, where most of the error sources might be canceled. To be further validated in near-future activities.

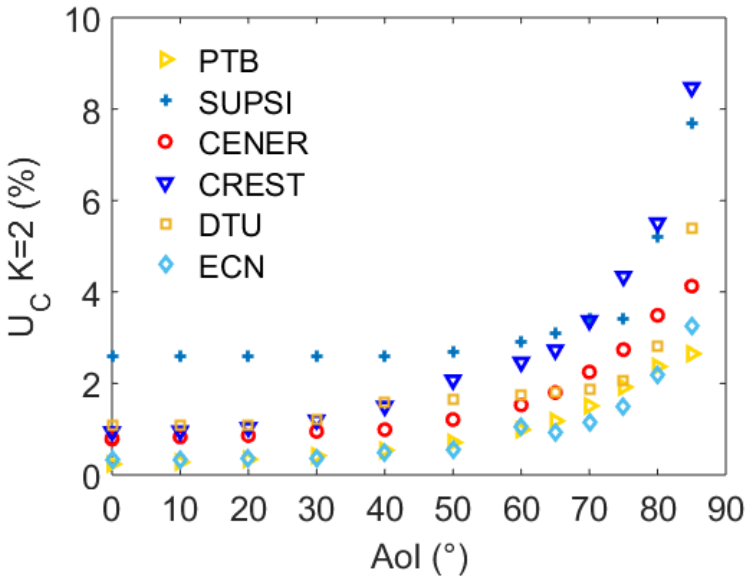

Figure 51: Expanded uncertainty from six laboratories as a function of AoI.

The difference between each lab's angular transmission measurement $\tau(\theta)$ and the reference value Xref is displayed in figure 52, where the reference value Xref is the weighted mean of all partner´s $\tau(\theta)$ defined as:

$$X_{ref} = \frac{\sum_{i=1}^{N} \frac{x_i}{\sigma_i^2}}{\sum_{i=1}^{N} \frac{1}{\sigma_i^2}}$$

where x_i is the individual laboratoty's relative transmissivity and σ_i is the $k = 1$ uncertainty of the lab's measurement. Here the measurements are weighted by the uncertainty provided by each partner. Note that relative differences above 4% in figure 52 have been removed from the plot in order to create a finer view of the y-axis. The agreement between measurements taken at Supsi and to the weighted mean is better than ±2% in the range of AoIs from -85° to +85°.

The assessment of the uncertainty estimation is done in term of the E_n score define as

$$E_n = \frac{x_i - X_{ref}}{\sqrt{UC_i^2 + UC_{ref}^2}}$$

where the numerator of E_n score is the deviation of the measured angular transmission from the reference (or assigned) value and the denominator is a combined expanded uncertainty, calculating UC_{ref} as:

$$UC_{ref} = \frac{2}{\sqrt{\sum_{i=1}^{N} \frac{1}{\sigma_i^2}}}$$

The interpretation of E_n can be twofold: $|E_n| > 1.0$ may indicate either a need to correct measurement issues and/or to review the uncertainty estimates.

The E_n score as a function of AoI for the Black-Si A sample is depicted in figure 53. Our measurements agree to the weighted mean within the stated uncertainties for the measurement angles in the full range of the measurements, from -85° to +85°.

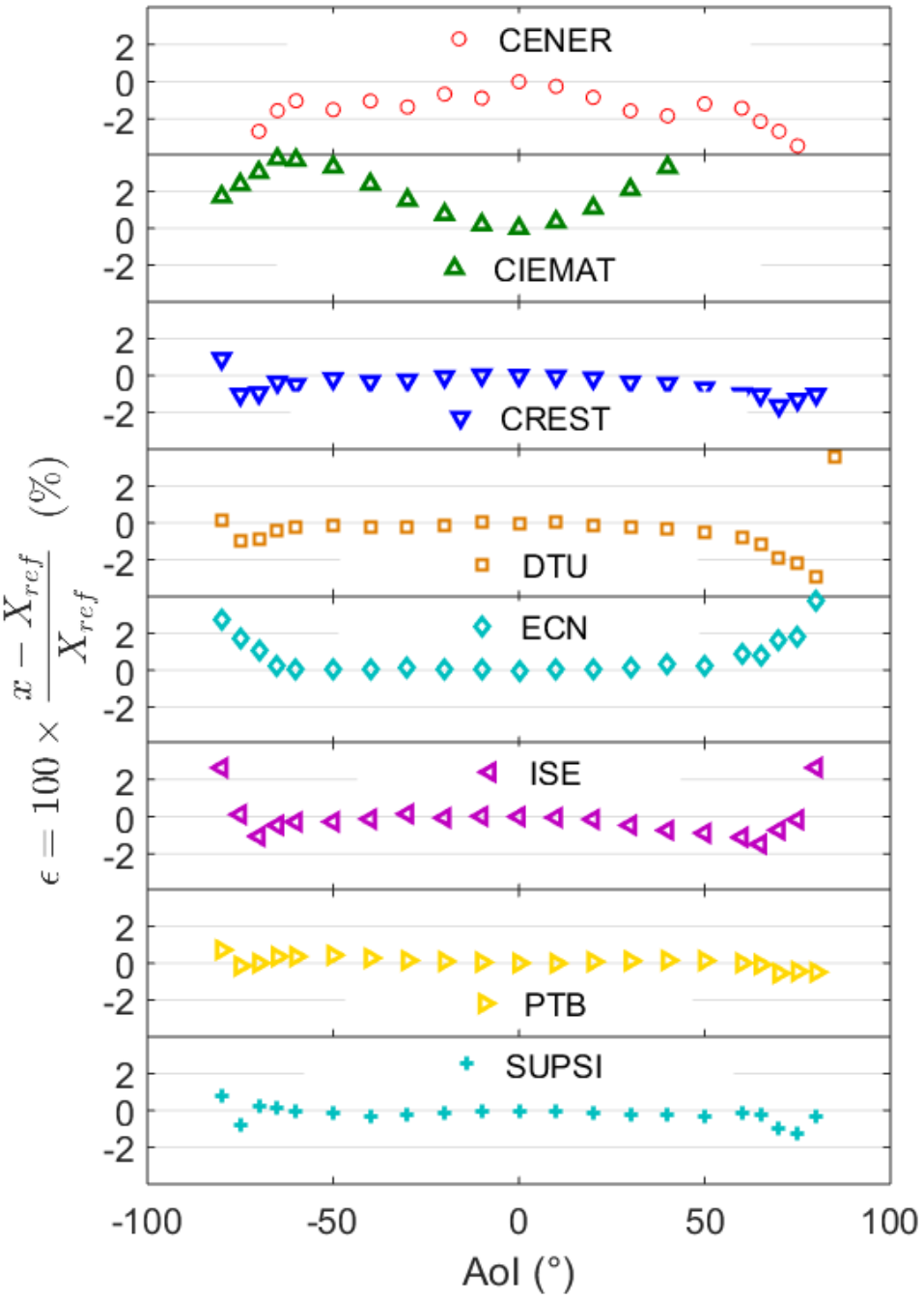

Figure 52: Plot showing the difference between each lab's measurement and the reference value Xref.

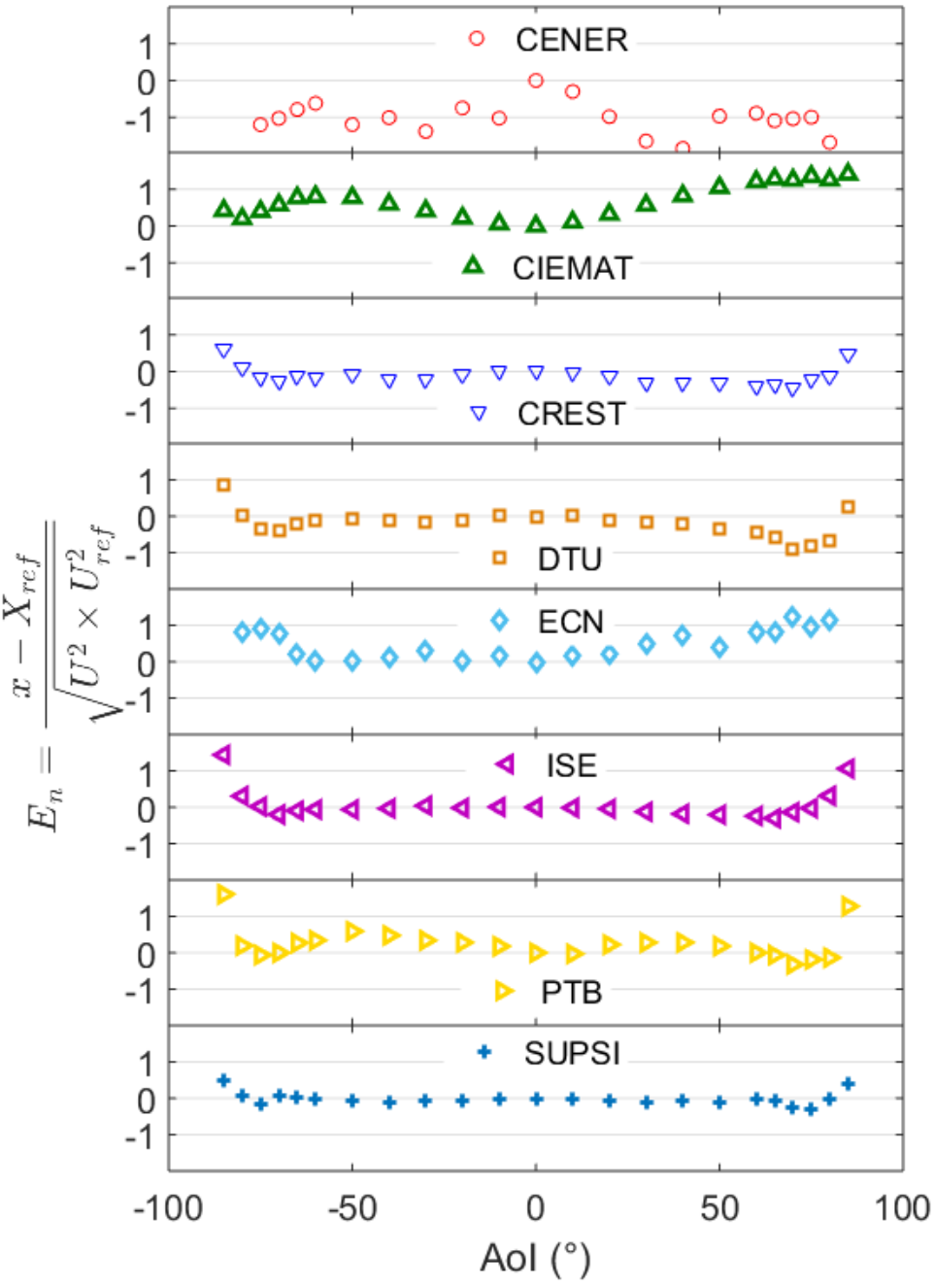

Figure 53: E_n number as a function of AoI θ for the measurements from eight laboratories.

3 Conclusions and outlook

The photovoltaic market is driven by the price per watt. The process of power rating is subject to measurement uncertainties and its economic impact is significant to the PV industry. In a scenario where the 27 IEA PVPS countries installed at least 83,4 GW in 2017 [IEA PVPS T1-34], every 1% of uncertainty would cost at least 417M€ per year assuming a nominal price of 0.5€/Wp in silicon modules.

This work focused to explore new test procedures and measurement uncertainty for new modules reaching the market promising either higher energy yields or added value due to aesthetics appearance and to support Swiss leading research institutes and module manufacturers. The conclusions drawn from developed activities and outlook are presented below:

- Highly capacitive modules begin to be widely present in the photovoltaic market. Their power measurement cannot be properly measured with just one single 10 ms flash and a linear voltage ramp. An accurate characterization requires a measurement method with either longer sweep-times or alternative methods with complicated recipes requiring customized voltage profiles or the execution of many flashes to measure a single IV-curve. The configuration of these recipes in a testing laboratory that measure several type modules is quite time consuming and therefore expensive. This technology remains a challenge for laboratories requiring accurate and cost-effective procedures.
- The power delivery from photovoltaic devices is a direct function of module temperature and incident irradiance. Matrices of module performance with respect to those ambient parameters are key input data for energy rating and shall be determined according to the standard IEC 61853-1. The procedure for indoor measurement of such matrices is not defined and standardized for bi-facial modules and requires further investigations.
- The incidence angle test described in the standard IEC 61853-2 dictates the fraction of irradiance available to be absorbed by PV devices at a particular incidence angle. The test method requires a light source with uniformity in the volume spanned by a full module upon rotation. This type of light sources is not typically available in size of commercial modules and the alternative foreseen in the standard method considers the use of a reduced test sample based on only one optically equivalent active. The facilities of most laboratories are then compatible with this type of measurement. However, indoor characterization of the incidence angle effect at module size remains a challenge and new or alternative measurement procedures should be developed.
- An increasing number of coloured modules are reaching the market promising added value due to better building integration and aesthetics. The energy yield of these module is significantly changing with customization of the product (layer position, colour/s, uniformity, transparency and opacity). The knowledge of short circuit dependencies as described by the spectral and angle of incidence response are not only important for the prediction of the performance of coloured modules, as demonstrated in this work, but also for an accurate characterisation with solar simulators. Compared to standard transparent c-Si modules the spectral mismatch error and angle of incidence effects have a higher impact on the measurement accuracy, requiring therefore further investigations. The brought customization of coloured modules makes it almost impossible to develop spectrally matched reference cell as usually used for the characterisation of standard modules. A further field of investigation is instead related to the long term stability of the coatings and its impact on module reliability.

4 Publications

Riedel 2018 N. Riedel, A.A. Santamaria Lancia, M. Amdemeskel, S. Thorsteinsson, P.B. Poulsen, F. Plag, I. Kröger, L.H. Slooff, M.J. Jansen, A.J. Carr, P. Manshanden, M. Bliss, T.R. Betts, I. Petrina Jauregui, M. Ezquer Mayo, J.L. Balenzategui, R. Roldán, U. Kräling, G. Baarah, B. Iandolo, R.S. Davidsen, A. Thorseth, C. Dam-Hansen, G.A. dos Reis Benatto, Interlaboratory Comparison of Methodologies for Measuring the Angle of Incidence Dependence of Solar Cells, EUPVSEC, 2018

Halwachs 2018 M. Halwachs, M. Rennhofer, R. Galleano, W. Zaaiman, M. Pravettoni, M. Theristis, A. Phinikarides, N. Riedel, A. Thorseth, M. Po, K. Hoogendijk, E. Haverkamp, A. Minuto, V. Tatsiankou, R. Roldán, M. Marzoli, I. Cole, D. Alonso-Álvarez, N. Ferretti, A. Drobisch, G. Belluardo, R. Fucci, M. Friederichs, Improvement of accuracy and precision of spectral irradiance measurements in annual spectroradiometer intercomparison, PVSEC, 2018.

Pravettoni 2018 M. Pravettoni, R. Galleano, W. Zaaiman, D.A. Alvarez, G. Belluardo, T.R. Betts, J.A. Bogeat, I. Cole, A. Drobisch, N. Ferretti, D. Friedrich, R. Fucci, T. Gómez, G. Graditi, M. Halwachs, E. Haverkamp, A. Minuto, A. Phinikarides, F. Plag, M. Rennhofer, R. Roldan; N. Riedel, M. Theristis, A. Thorseth, G. Timò, J.M. Vilaplana, Spectroradiometry in PV: how inter-laboratory comparison may improve measurement accuracy, WCPVEC, 2018.

Friesen 2019 G. Friesen, R. Roldan Molinero Energy Yield of coloured PV modules in the field. EUPVSEC 2019.

5 References

Chang 2018 — S. Chang, Y. Choe, H. Cho, H.J. Park, Ch. Reise, G. Baarah, E. Schnabel, U. Kräling, B. Müller, „Annual outdoor performance of LG bifacial modules, 5th bifiPV Workshop 2018, Denver, CO.“

Deline 2017 — C. Deline, S. MacAlpine, B. Marion, F. Toor, A. Asgharzadeh and J. S. Stein, Assessment of Bifacial Photovoltaic Module Power Rating Methodologies – Inside and Out, IEEE Journal of Photovoltaics 7, 2, 2017.

EN50380 — EN50380:2017-09, Marking and documentation requirements for Photovoltaic Modules, European Committee for Electrotechnical Standarization, Brussels, 2017.

Engelhart 2011 — P. Engelhart, D. Manger, B. Klöter, S. Hermann, A. Stekolnikov, S. Peters, H. Ploigt, A. Eifler, C. Klenke, A. Mohr, G. Zimmermann, B. Barkenfelt, K. Suva, J. Wnedt, T. Kaden, S. Rupp, D. Rychtarik, M. Fischer, J. Müller and P. Wawer, “Q.ANTUM-Q-Cells next generation high-power silicon cell & Module concept”, EUPVSEC, 2001

Hohl-Ebinger 2011 — Jochen Hohl-Ebinger and Wilhelm Warta, uncertainty of the spectral mismatch correction factor in STC measurements on photovoltai devices, Prog. Photovolt. Res. Appl. 19, 573, 2011.

IEA PVPS T1-34 — International Energy Agency (IEA). Trends 2018 in photovoltaic applications. Report IEA PVPS T1-34:2018.

IEC 61724-1 — IEC 61724-1: 2017, Photovoltaic system performance – part 1: Monitoring, Bureau Central de la Comission Electrotechnique Internationale, Ginebra, 1987.

IEC 61853-3 — IEC 61853-3:2018, Module performance testing and energy rating. Part 3: Energy rating of PV modules, Bureau Central de la Comission Electrotechnique Internationale, Ginebra, 1987.

IEC 60904-1-2 — IEC TS 60904-1-2:2019, Photovoltaic devices. Part 1-2: Measurement of current-voltage characteristics of bifacial photovoltaic (PV) devices, Bureau Central de la Comission Electrotechnique Internationale, Ginebra, 1987.

Ishii 2011a — T. Ishii, T. Takashima and K. Otani, Long-term performance degradation of various kinds of photovoltaic modules under moderate climatic conditions, Prog. Photovolt. Res. Appl. 19,141, 2011.

Ishii 2011b — T. Ishii, K. Otani and T. Takashima, Effects of solar spectrum and module temperature on outdoor performance of photovoltaic modules in round-robin measurements in Japan, Prog. Photovolt. Res. Appl. 19,170, 2011.

Merten 1998a — J. Merten, J. M. Asensi, C. Voz, A. V. Shah, R. Platz and J. Andreu, “Improved equivalent circuit and analytical model for amorphous silicon solar cell and modules”, IEEE Trans. Electron Devices ED-45, 423,1998.

Münzer 2011 — K. Münzer, J. Schöne, A. Teppe, M. Hein, R. E. Schlosser, M. Hanke, K. Varner, H. Mäckel, S. Keller and P. Fath,“Physical properties of industrial 19% rear side passivates Al-LBSFR-solar cells“, Energy Procedia, 8, 415, 2011.

Riedel 2018 — N. Riedel, A.A. Santamaria Lancia, M. Amdemeskel, S. Thorsteinsson, P.B. Poulsen, F. Plag, I. Kröger, L.H. Slooff, M.J. Jansen, A.J. Carr, P. Manshanden,

M. Bliss, T.R. Betts, I. Petrina Jauregui, M. Ezquer Mayo, J.L. Balenzategui, R. Roldán, U. Kräling, G. Baarah, B. Iandolo, R.S. Davidsen, A. Thorseth, C. Dam-Hansen, G.A. dos Reis Benatto, Interlaboratory Comparison of Methodologies for Measuring the Angle of Incidence Dependence of Solar Cells, EUPVSEC, 2018.

Schwab 2012 C. Schwab, A. Wolf, M. Graf, J. Nekarda, G. Kästner, M. Zimmer, S. Kühnhold, M. Hofmann, D. Biro and R. Preu, “Passivation of inline wet chemical polished surfaces for industrial PERC devices “, Energy Procedia, 27, 573, 2012.

Singh 2012 J. P. Singh, T. M. Walsh, A. G. Aberle, “Performance investigation of bifacial PV modules in the tropics”, EUPVSEC, 2012.

Sugibuchi 2013 K. Sugibuchi, N. Ishikawa, S. Obara, “Bifacial-PV Power Gain in the Field Test Using “EarthON” High Bifaciality Solar Cells”, UEPVSEC, 2013.

Stodolny 2016 M.K. Stodolny, M. Lenes, Y. Wu, G.J.M. Janssen, I.G. Romijn, J.R.M. Luchies, L.J. Geerligs, “n-Type polysilicon passivating contact for industrial bifacial n-type” Solar Energy Materials and Solar Cells, 158, 24, 2016.

Taguchi 2014 M. Taguchi, A. Yano, S. Tohoda, K. Matsuyama, Y. Nakamura, T. Nishiwaki and E. Maruyama, “24.7% record efficiency HIT solar cell on thin film silicon wafer”, IEEE J. Photovolt. 4, 96, 2014.